Geophysical Journal International

Geophys. J. Int. (2016) **207,** 589–607
Advance Access publication 2016 August 8
GJI Seismology

doi: 10.1093/gji/ggw294

An investigation into the bedrock depth in the Eskisehir Quaternary Basin (Turkey) using the microtremor method

M. Tün,[1] E. Pekkan,[1] O. Özel[2] and Y. Guney[1]

[1]*Earth and Space Sciences Institute, Anadolu University, Eskişehir, Turkey. E-mail: mtun@anadolu.edu.tr*
[2]*Faculty of Engineering, Istanbul University, Istanbul, Turkey*

Accepted 2016 August 2. Received 2016 August 2; in original form 2015 December 27

SUMMARY

Amplification can occur in a graben as a result of strong earthquake-induced ground motion. Thus, in seismic hazard and seismic site response studies, it is of the utmost importance to determine the geometry of the bedrock depth. The main objectives of this study were to determine the bedrock depth and map the depth-to-bedrock ratio for use in land use planning in regard to the mitigation of earthquake hazards in the Eskişehir Basin. The fundamental resonance frequencies (f_r) of 318 investigation sites in the Eskişehir Basin were determined through case studies, and the 2-D *S*-wave velocity structure down to the bedrock depth was explored. Single-station microtremor data were collected from the 318 sites, as well as microtremor array data from nine sites, seismic reflection data from six sites, deep-drilling log data from three sites and shallow drilling log data from ten sites in the Eskişehir Graben. The fundamental resonance frequencies of the Eskişehir Basin sites were obtained from the microtremor data using the horizontal-to vertical (H/V) spectral ratio (HVSR) method. The phase velocities of the Rayleigh waves were estimated from the microtremor data using the spatial autocorrelation (SPAC) method. The fundamental resonance frequency range at the deepest point of the Eskişehir Basin was found to be 0.23–0.35 Hz. Based on the microtremor array measurements and the 2-D *S*-wave velocity profiles obtained using the SPAC method, a bedrock level with an average velocity of 1300 m s^{-1} was accepted as the bedrock depth limit in the region. The log data from a deep borehole and a seismic reflection cross-section of the basement rocks of the Eskişehir Basin were obtained and permitted a comparison of bedrock levels. Tests carried out using a multichannel walk-away technique permitted a seismic reflection cross-section to be obtained up to a depth of 1500–2000 m using an explosive energy source. The relationship between the fundamental resonance frequency in the Eskişehir Basin and the results of deep drilling, shallow drilling, shear wave velocity measurement and sedimentary cover depth measurement obtained from the seismic reflection section was expressed in the form of a nonlinear regression equation. An empirical relationship between f_r, the thickness of sediments and the bedrock depth is suggested for use in future microzonation studies of sites in the region. The results revealed a maximum basin depth of 1000 m, located in the northeast of the Eskişehir Basin, and the SPAC and HVSR results indicated that within the study area the basin is characterized by a thin local sedimentary cover with low shear wave velocity overlying stiff materials, resulting in a sharp velocity contrast. The thicknesses of the old Quaternary and Tertiary fluvial sediments within the basin serve as the primary data sources in seismic hazard and seismic site response studies, and these results add to the body of available seismic hazard data contributing to a seismic microzonation of the Eskişehir Graben in advance of the severe earthquakes expected in the Anatolian Region.

Key words: Surface waves and free oscillations; Site effects.

1 INTRODUCTION

To fully understand the seismic risk associated with a region, we must first understand the effects of the regional 2-D/3-D underground structure on wave propagation. Seismic waves penetrating from the source into the basin structure at lower velocities and densities are balanced by an increase in the amplitude of the wavelength, which shortens as a result of differences in acoustic impedance (Lanzo & Silvestri 1999; Field & Group 2000). In addition, seismic waves that propagate in the ground lose some of their elastic energy as a result of attenuation in the form of plastic deformation. The other factors in soil amplification are the lower limit of the basin structure, the geometry of the sediment–bedrock interface, and resonance effects (Field & Group 2000). Seismic waves are affected by local soil conditions, which have a direct impact on the potential consequences of an earthquake. The identification of risks (through studies of expected seismic hazards and risk mitigation) is carried out within the context of risk management, with hazard analysis being one of the most important factors in disaster mitigation. The seismicity of an area makes the determination of the bedrock geometry a primary parameter in studies of seismic soil response and seismic hazard.

Eskişehir, a city in the west of the Central Anatolian Region, is undergoing rapid urbanization and industrialization, so a major earthquake would result in significant financial losses, as well as damage to morale, due to the high population, large-scale industrial production, and socio-economic conditions. A major earthquake would also have significant adverse effects on the city's industrial contribution to the national economy. The 2014 census put Eskişehir's population at 812 320. Eskişehir Plain becomes significantly narrower towards Gökdere in the east and extends to the Alpu Plain as a narrow belt. Shuttle Radar Topography Mission (SRTM) data show that the elevation of the study area varies between 780 and 1200 m.

The largest watercourse in the area is the Porsuk River, which enters from the southwest and leaves from the east. The Sarisu Creek flows from west to east and joins the Porsuk River (Fig. 1). Despite higher elevations to the north and south of the study area, the middle section, where most of the settlement is concentrated, is rather flat. These lowlands, referred to as the Eskişehir Plain, open onto the Alpu Plain in the east and the İnönü Plain in the west. The study area shown framed in black in Fig. 1 is 35 km long from east to west and 20 km long from north to south.

The main aim of this study was to develop a fundamental approach to determining the bedrock depth in the Eskişehir Basin, which would be a key piece of information in studies related to hazard assessment. Hazards generate from expected ground motions in a seismic event can typically be obtained using instrumental records. Horizontal-to vertical (H/V) ratios based on ambient noise records (Nogoshi & Igarashi 1971; Nakamura 1989) and dispersion curves obtained from array records (Aki 1957; Horike 1985) were used to estimate the shear wave velocity profile. For the deep basins, *P*-wave velocity profiles can be obtained without much difficulty using explosives or large vibrators, but the situation is significantly different in the case of *S*-wave velocity profiles. When the depth to the basement in a large basin exceeds 4–5 km, it is quite difficult to obtain *S*-wave velocity profiles by means of a seismic survey using *S*-wave generators. That said, array observations of microtremors, such as the spatial autocorrelation (SPAC) method (Aki 1957; Okada 2003), make it possible to estimate *S*-wave velocity profiles beneath arrays with no controlled sources by inverting the phase velocity dispersions of surface waves (Horike 1985). Array observations of microtremors yield *S*-wave velocity profiles at a lower cost than other seismic surveys. A secondary aim of the study was to explore the 2-D *S*-wave velocity (V_s) structure down to bedrock depth, and to this end, V_s models were obtained using microtremor array records. Regional variations in the results were investigated using a geographical information system interface and geostatistical methods, and conclusions were drawn based on the overall trends.

The H/V spectral ratios (HVSRs) of the recorded horizontal and vertical components were calculated using ambient noise records in an evaluation of the fundamental resonance frequency. The H/V ratio microtremor method has become popular worldwide since it was proposed by (Nakamura 1989), and its advantages and limitations have been discussed at length in the literature (Lachetl & Bard 1994; Kudo 1995; Bard 1998; Bard & SESAME Team 2005; Bonnefoy-Claudet *et al*. 2006; Parolai *et al*. 2009).

Using the H/V spectral ratio (Nakamura) method, HVSRs were studied using microtremor records to determine the fundamental resonance frequency. A total of 318 single-station microtremor measurements were conducted to investigate the structure of the Eskisehir Basin. Then, using a seismic reflection method, deep borehole data, and a microtremor array, the SPAC method was used to determine the relationship between sediment thickness and the f_r values obtained using the HVSR method. Several seismic reflection surveys have been carried out in the Eskişehir Basin using P-Gun that have partially covered the new alluvium, and the bedrock depths and sediment thicknesses have been observed for four different locations in the Eskişehir Basin. The results obtained from active- and passive-source shallow seismic methods were compared with deep drilling data, and with the shear wave velocity values obtained using microtremor array techniques. The aim of these comparisons was to explore the relationship between the sediment thickness and the fundamental resonance frequency calculated using the HVSR method. The findings related to this relationship were used to determine the bedrock depth for locations where the resonance frequency is known but for which no deep borehole data, seismic reflection data, or microtremor array data were available. Finally, the geometry of the bedrock depth structure of Eskisehir basin is presented to provide detailed information about seismic hazards for use in future seismic site response studies.

1.1 Geology and seismicity of the area

The seismicity map for the study area and its surroundings and the location of the 20/02/1956 ($M_s = 6.4$) Eskişehir Earthquake are presented in Fig. 1(a). The seismicity map of Turkey indicates that Eskişehir is located in a 2nd-degree earthquake zone (PGA_{rock}: 0.3–0.4 g; Earthquake Zonation Map of Turkey; AFAD 1996), meaning that the seismic hazard level is considered low and potential risks are minor. However, in the city of Eskişehir, medium-magnitude earthquakes (between $M = 5$ and $M = 7$) have occurred in the past, with 15 earthquakes of $M \geq 4$ recorded in the 20th century. The strongest event detected in Eskişehir, according to instrument recordings, occurred on 1956 February 20, when an earthquake of magnitude $M_s = 6.4$ hit the region (McKenzie 1972), although the epicentre of the main shock is still a matter of some debate in the related literature (Ocakoğlu & Açikalin 2010). Some researchers argue that the right–lateral fault has been superimposed by a younger normal fault system (Gözler *et al*. 1985; Yaltirak 2002; Koçyiğit 2005; Ocakoğlu 2007), while others suggest that strike–slip faults dominate the region's seismicity (Altunel & Barka 1998; Şaroğlu

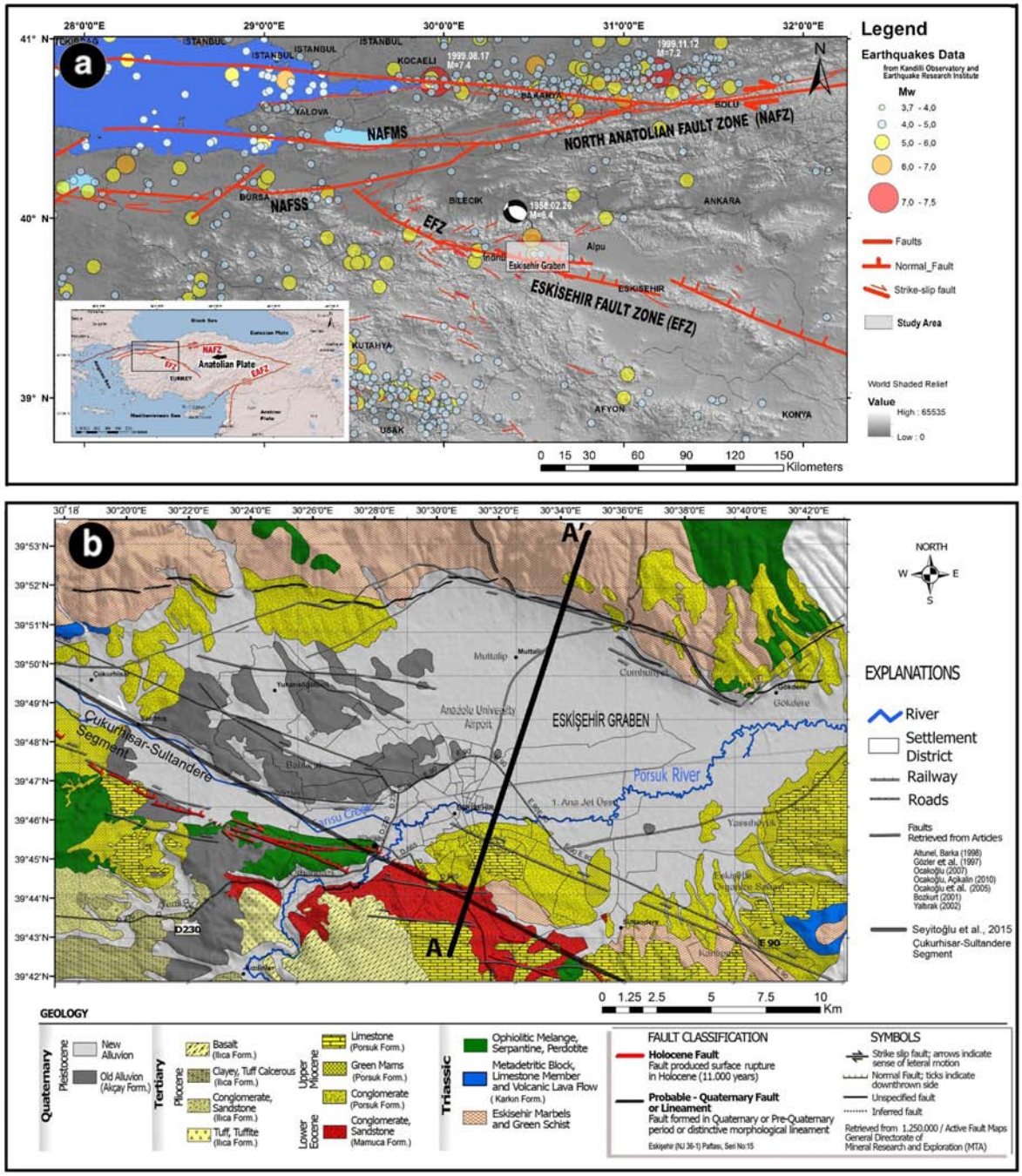

Figure 1. (a) Active tectonic regions in Turkey and active fault segments in Central Anatolia. Retrieved from Koçyiğit & Özacar (2003) and Ocakoğlu (2007). (b) Generalized geological map of the study area. Retrieved from Altunel & Barka (1998), Yaltirak (2002), Şaroğlu *et al*. (2005), Ocakoğlu (2007), Orhan *et al*. (2007), Emre *et al*. (2013) and Seyitoğlu *et al*. (2015).

et al. 2005; Seyitoğlu *et al*. 2010; Tün *et al*. 2010; Seyitoğlu *et al*. 2015). The Eskisehir Fault Zone is one of the major neotectonic structures of Turkey, extending from Bursa, İnegöl to Cihanbeyli; see Fig. 1(a); see also (Yaltirak 2002; Dirik & Erol 2003; Tokay & Altunel 2005; Ocakoğlu 2007; Emre *et al*. 2013). The formations within the boundaries of the city of Eskişehir are, in order from the youngest to the oldest, alluvium, the Akçay Formation, the Ilica Formation, the Porsuk Formation, the Mamuca Formation and the Karkin Formation (Pekkan *et al*. 2015; Fig. 1b). The 1500-km-long North Anatolian Fault Zone (NAFZ) is divided into three fault segments to the east of the Marmara Sea (Emre *et al*. 2013). The northern segment, which is the central strand of the North Anatolian Fault (NAFMS), extends in an east–west direction through Iznik Lake, Gemlik Bay and Bandirma Bay, after which it turns southwestwards, entering a fault zone that is formed by the many faults around the western part of Bandirma Bay. The southern segment of the North Anatolian Fault (NAFSS) runs in a northeast–southwest direction, extending from Pamukova. The NAFSS stretches from Bursa to Manyas, follows the southwestern coast from the southern coast of Uluabat Lake, and reaches the southern part of Manyas Lake with a WNW–ESE orientation (Fig. 1; Sengör *et al*. 1985; Yaltirak 2002). The A–A′ profile in Fig. 1 shows the sediment–bedrock

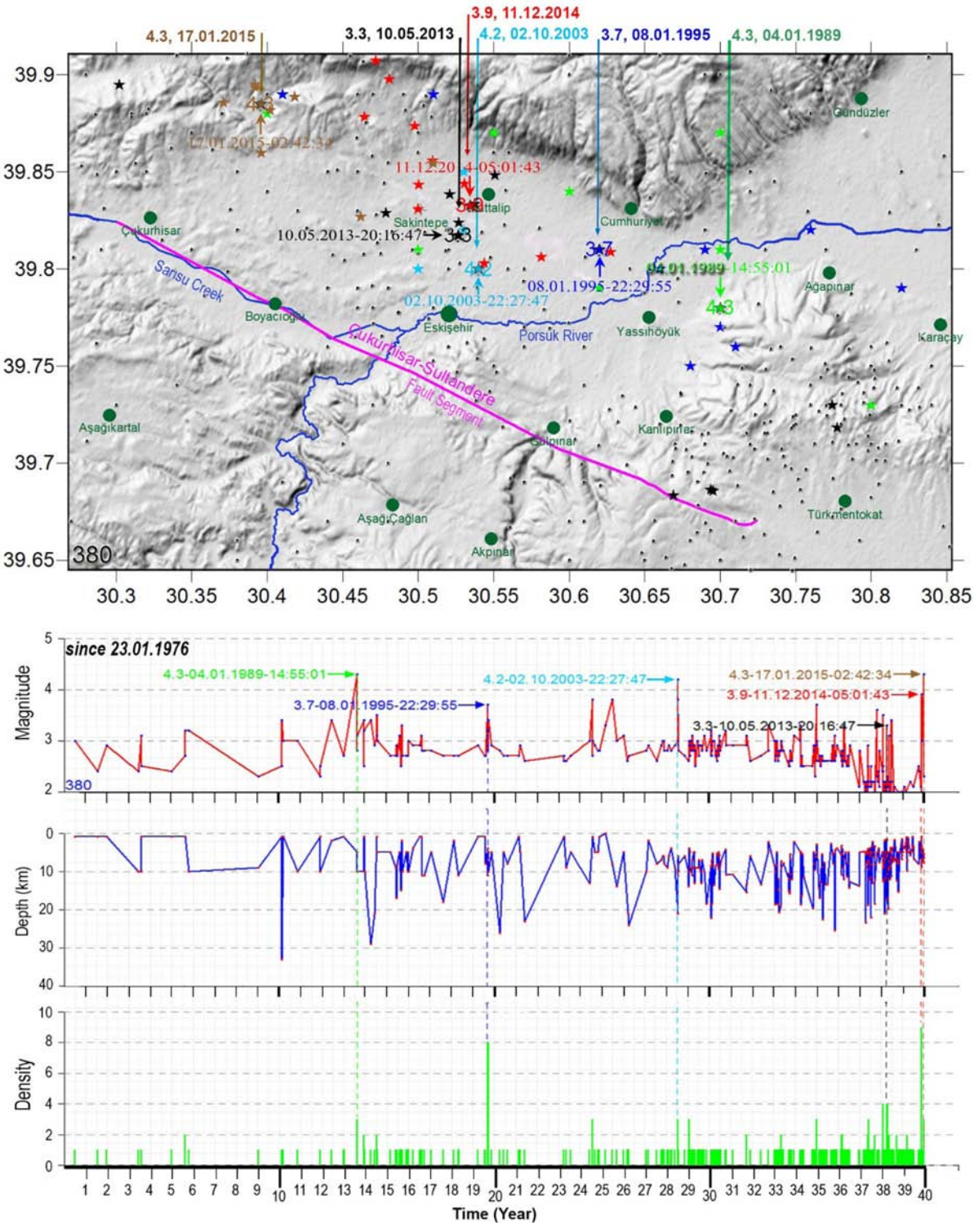

Figure 2. Location and size of earthquakes that have occurred within the Eskişehir Graben since 1976 January 23.

thickness calculated from the HVSR curve f_r values described in the next section. The Eskişehir Fault that commences to the west of Bursa extends to Sivrihisar in the east, according to Barka *et al.* (1995), who attributed significant regional importance to the fault and argued that it is the major geological element separating Central Anatolia, characterized by strike–slip faults from Western Anatolia, from the Aegean Region, where dilatation occurs with larger and regular faults. It was (Altunel & Barka 1998) who first defined this fault, extending from Bursa to Kaymaz, as the 'Eskişehir Fault Zone' (EFZ; Fig. 1b). There have been 380 earthquakes in the Eskişehir Graben since 23 January 1976 (Fig. 2). The size, depth, and density diagrams of these earthquakes are shown in Fig. 2.

The Eskişehir Basin features gravel from the Pleistocene era, sand, silt, clay-like alluvium, the Akçay Formation, conglomerate sandstone, marl, the Porsuk Formation from the Late Miocene era with limestone and basalt, tuff, clay-like tuff limestone and the Ilica

Formation from the Pliocene era with conglomerate sandstone. The Porsuk Formation contains clay-like tuff belonging to the Pliocene Ilica Formation outcrops at calcareous levels (Fig. 1b).

2 DATA AND RESULTS

2.1 HVSR method

Microtremors can be defined as seismic vibrations that result from either anthropic or natural causes and that vary over daily or weekly periods (Bonnefoy-Claudet *et al*. 2004; Cornou *et al*. 2004). Anthropogenic noise results from such local human activities as industry, traffic and construction, which typically produce seismic energy in the frequency band of 2–50 Hz. Natural noise, on the other hand, results in seismic vibrations formed on a local scale due to the interaction of such events as wind and storms with structures on land, as well as ocean waves, watercourses and lakes. Microtremors occur in the 0.2–2 Hz frequency band, and the seismic wave zones they create include both body waves and higher-mode surface modes. The microtremor method is widely used to determine the fundamental resonance frequencies (f_r), bedrock depth and shear wave velocity (V_s) of the sedimentary layers on the bedrock.

In the HVSR method, the spectral ratio between the horizontal component and the vertical component is determined using a technique based on research by (Omori 1908) and further developed by Kanai (Kanai *et al*. 1954; Kanai 1961; Kanai & Tanaka 1961) and (Nogoshi & Igarashi 1970; Nogoshi & Igarashi 1971). The H/V method gained wider popularity after Nakamura's work (Nakamura 1989), as Nakamura's method provides a dependable value for the fundamental resonance frequency of a site (Konno & Ohmachi 1998). Theoretical (Bard 1998) and experimental (Lermo & Chávez-García 1994) studies based on peak values obtained from microtremor measurements and H/V spectral ratios have revealed that the method is suitable for use in determining the local fundamental resonance frequency but cannot safely identify ground motion amplification rates due to geological structures. These studies have shown that the peaks in HVSR curves result from large impedance contrasts between soft sediments and bedrock. The determination of the fundamental resonance frequency of a site is considered to be primary data related to the site effects for residential areas, and it can also be related to the thickness of soft sediments (Delgado *et al*. 2000; Parolai *et al*. 2002; Özalaybey *et al*. 2011).

2.2 HVSR observations

Ambient noise measurement studies were carried out in the Eskişehir Basin from June 2010 to the spring of 2012. The collection of microtremor data, the data processing, and the interpretation of the H/V curves were completed following the guidelines and recommendations of the SESAME (Site EffectS assessment using AMbient Excitation) Consortium (Atakan *et al*. 2004; Bard & SESAME 2005; Wathelet 2005; Di Giulio *et al*. 2006; Wathelet 2007). In this study, single-station microtremor measurements were carried out at 318 points to create a 3-D model of the Eskişehir Basin and determine the fundamental resonance frequency of the basin's sedimentary overburden. Microtremor data were recorded using a Guralp CMG-6TD-series recording system. At some of the measurement points, CMG-6TD sensors were sited in 30-cm-deep pits to prevent the results from being influenced by long-period noises produced by high winds. A microtremor measurement approximately 1 hr in duration was taken at each point and recorded at a 100-sps sampling interval.

A module of the open-source Geopsy software package, developed as part of the SESAME European Project (Bard & SESAME Team 2005; Wathelet *et al*. 2008), was used to process the microtremor data at all measurement points. Moreover, as part of the framework of (Bard & SESAME Team 2005) studies, the *reliability conditions* were itemized while calculating the H/V curves.

The H/V ratios were calculated at frequency intervals of 0–20 Hz. The spectral ratio graphic showed HVSR curves with single, double, or wide peaks in the range of 0–20 Hz. Flat HVSR curves were interpreted as 'no-peak' curves. Fig. 3 shows the variation of the HVSR curves obtained from the recordings within areas where the settlement is dense. The single-station microtremor data are concentrated within the settlement-intensive area at 500-m intervals, whereas the interval is in the range of 1–2 km for the other parts of the study area.

The results were interpreted using the first peak values in the H/V spectral ratios obtained from the microtremor measurements. In most of the microtremor measurements, a second peak value can be observed. In Fig. 4, exemplary H/V spectral ratio curves are given for five different locations.

As seen in examples A18, E13, H8 and G3 shown in Fig. 11, although almost of the second peaks are observed in the new alluvium (light grey colour) units, in example E2, no second peak can be seen in the H/V spectral ratio curves in the old alluvium (dark grey) units. These second peaks, which vary within the range of 4–8 Hz, are considered to be related to the upper-level soil layer, which is composed of modern sediments of the Eskişehir Plain, and the clasts accumulated by the Porsuk River and Sarisu Creek that joins the Porsuk River to the west of Eskişehir, which is referred to as the new alluvium unit in the literature. The H/V spectral ratios could not safely identify the ground motion amplification rates. We determined the H/V peaks of amplitudes 3–9 at frequencies of approximately 0.2–12 Hz.

2.3 Microtremor data and fundamental resonance frequency map of the Eskişehir Basin

The fundamental resonance frequency values were determined based on an HVSR analysis of single-station microtremor measurements obtained at 318 points (Fig. 5). The peak frequency values obtained were divided into five classes in the 0.2–20 Hz interval range and colour-mapped accordingly. The measurement points without a peak are indicated in black in Fig. 5. The spatial variations of the peak frequency values were colour-mapped over a 2-D plane using geostatistical methods (Fig. 5).

Ibs-von Seht & Wohlenberg (1999) showed that the fundamental resonance frequency (f_r) of a soil layer is closely related to the sediment thickness (h) through a relationship that can be established using a nonlinear regression model of the following form:

$$h = a f_r^{-b} \tag{1}$$

where a and b are unknown regression coefficients. The basis for this relationship comes from the simple formulation between the f_r of a flat-lying sediment layer with an average shear velocity of V_s and the thickness h overlying a hard-rock basement, which is expressed as $f_r = V_s/4h$ using the quarter-wavelength approach (Lachetl & Bard 1994; Ibs-von Seht & Wohlenberg 1999).

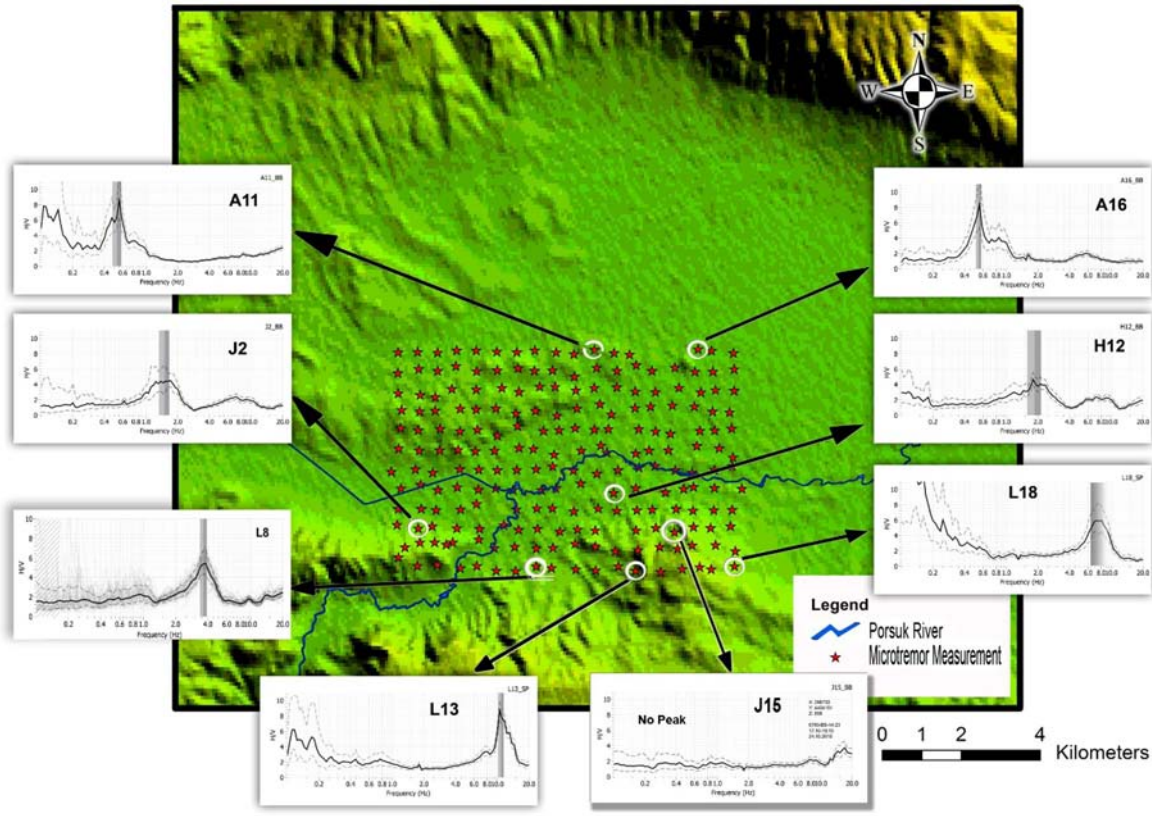

Figure 3. Spectral amplitudes of certain microtremors recorded at different locations in the Eskişehir Basin.

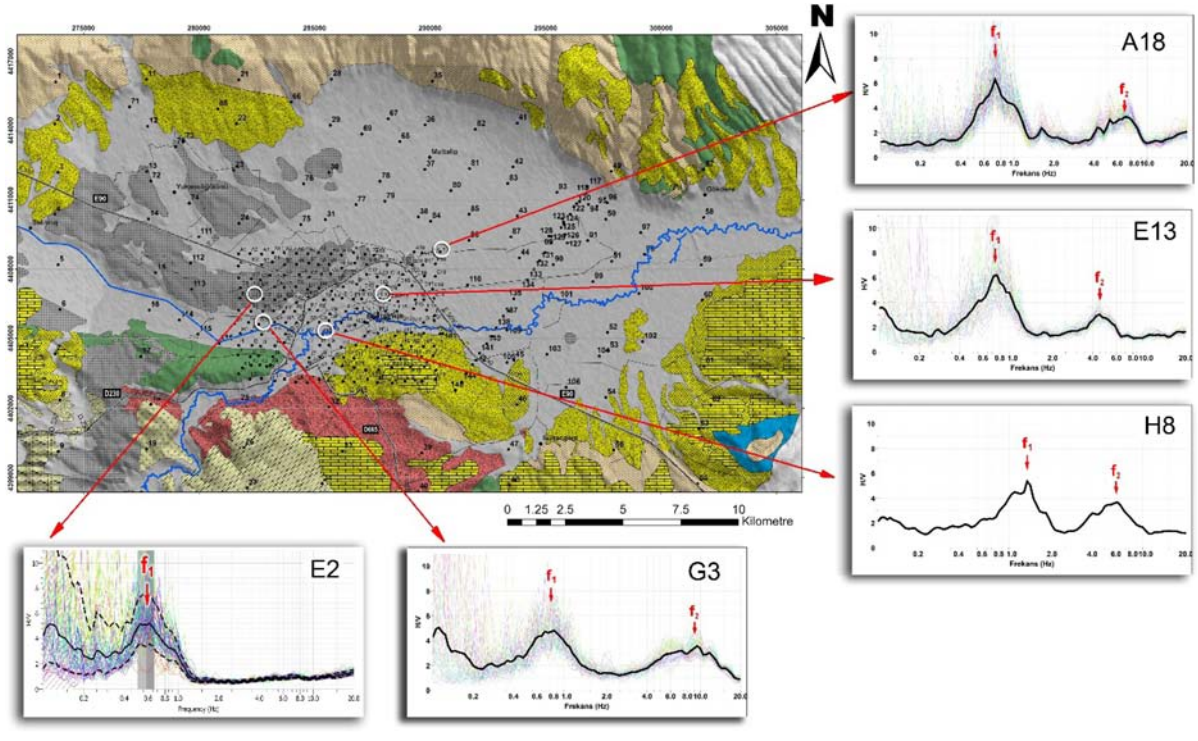

Figure 4. Map of microtremor measurement points within the study area and examples of H/V spectral ratio curves with and without a second peak.

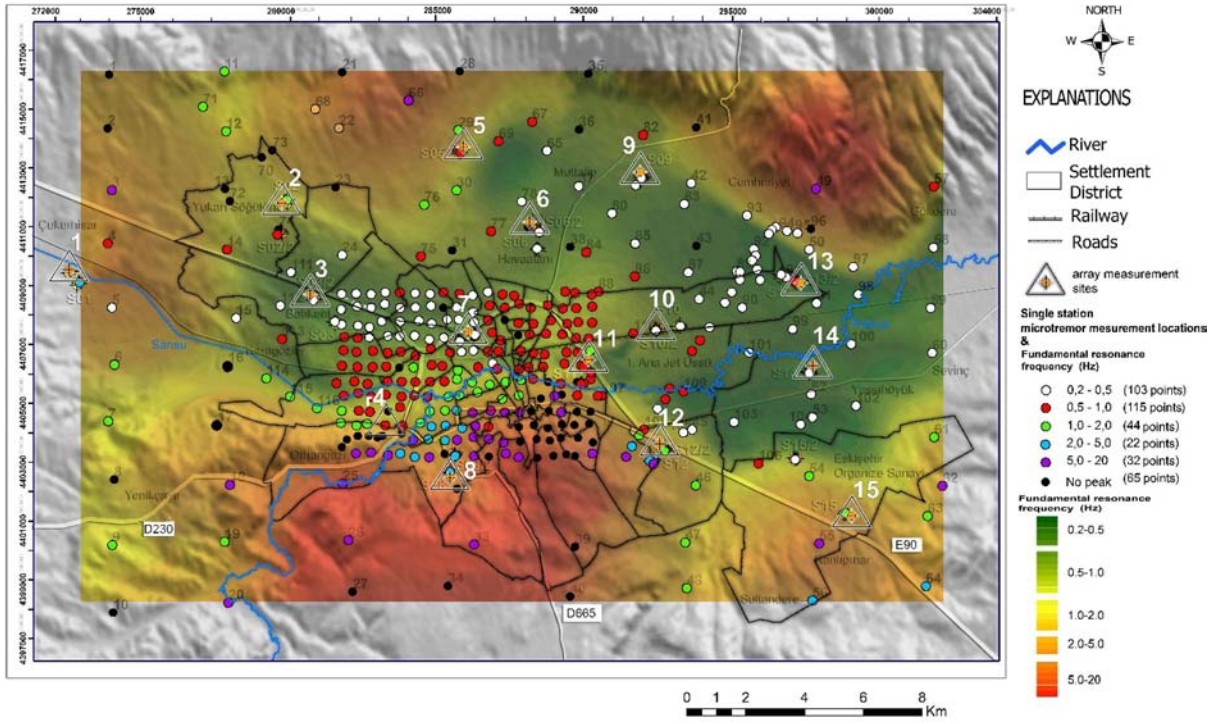

Figure 5. Map showing the locations of microtremor measurements and the fundamental resonance frequency values in the study area. Sites labelled with black-coloured alphanumeric letters indicate the locations of the microtremor measurements.

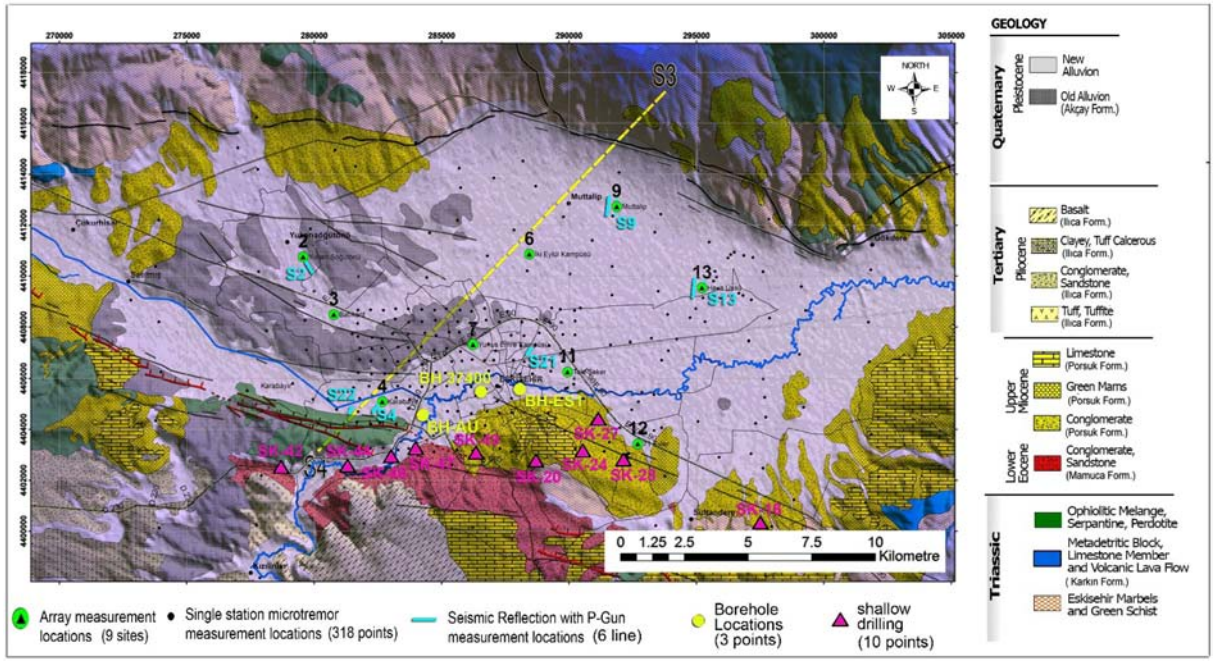

Figure 6. Numeric coding of nine microtremor array measurements, three deep boreholes, six seismic reflections, and ten shallow drilling sites on a geological map of the study area.

3 DETERMINATION OF THE DEPTH TO BEDROCK

The relationship between the top sediment thickness and the fundamental resonance frequency (f_r) was identified, and a function was developed to describe the relationship between the Eskişehir Basin bedrock depth and f_r using borehole data, seismic reflection data, and array observations of microtremors (using the SPAC method). In this study, deep borehole data (from two sties), MAM data (from nine sites), reflection surveys (from eight sites) and shallow drilling data (from ten sites) were used to calculate the sediment thickness. The sites are shown in Fig. 6.

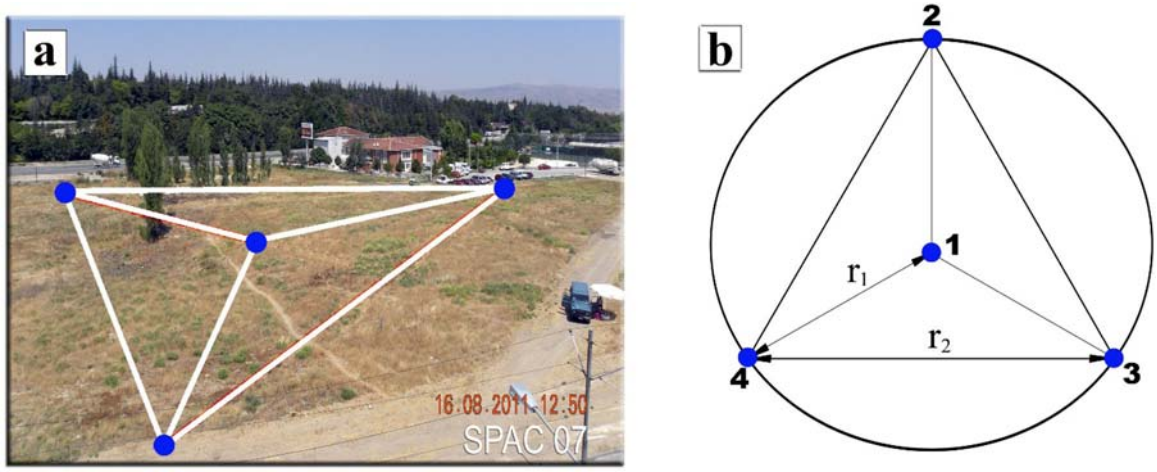

Figure 7. (a) Example of triangle configuration at MAM location 7 (r_1:90 m, r_2:155.88 m). (b) Instrumental array for the four-station 'triangle' array geometry used in this study. The numbers indicate accelerometer locations.

3.1 Microtremor observations and array measurements of microtremors

The microtremor array method (MAM) can be used to estimate Rayleigh wave dispersion curves using three component recordings of the ambient noise wave field (Aki 1957, 1965; Tokimatsu 1997; Köhler *et al*. 2007; Tada *et al*. 2009). We conducted array-based spatially averaged coherency (SPAC) microtremor measurements at nine sites to estimate the geometry of the sediment–bedrock interface. This method was used to evaluate the shear wave velocity structure above the deepest point of the basin (Okada 2003). The *S*-wave velocity structure was then estimated from an inversion of the phase velocities. The SPAC method can be used to extract the phase velocities of surface waves with modes of propagation that are different from those indicated by microtremor array observations. While the higher mode propagates faster than the fundamental mode, the fundamental mode has the lowest velocity. We assumed that microtremors are mainly composed of surface waves and that the fundamental mode of a surface wave is dominant. The most important advantages of the SPAC method are considered to be the ring array geometry, based on its easy-to-use *in situ* nature, with a minimum of at least four receivers, and the fact that it provides high-resolution information while determining the phase velocity at low frequencies (Okada 2003).

The application described in the following section deals only with vertical-component seismic measurements, and the discussion is limited to (dispersive) Rayleigh wave motion. Assuming that, for each frequency, the wave energy propagates at only one (scalar) velocity, it can be shown (Aki 1957; Asten 1976; Okada 2003) that the azimuthally averaged coherency for a ring array can be expressed as follows:

$$\bar{c}(f) = J_0(kr) = J_0\left(\frac{2\pi f r}{V(f)}\right), \tag{2}$$

where f is the frequency, $\bar{c}(f)$ is the azimuthally averaged coherency, J_0 is the zero-order Bessel function, K is the scalar wavenumber, $V(f)$ is the velocity dispersion function, and r is the inter-station distance (station separation) in the ring array. Theoretical coherencies are determined by first computing dispersion curves charted by phase velocity versus frequency for Rayleigh waves, using routines (Herrmann 2001), and then computing a model coherency spectrum using eq. (2). The radius planning depends on the target depth and the power of the circumferential microtremors. A high autocorrelation is anticipated between the microtremor records measured by stations within the array that are at equal distances from one another. A Rayleigh wave dispersion curve was produced by merging all of the dispersion curves obtained for each ring array.

In practice, the SPAC method requires a circular array consisting of three or more circumferential stations and one station at the centre of the circle (Okada 2006). In this study, to identify how the velocities of the *S*-waves in the Eskişehir Basin vary with depth and to investigate the basin structure, the array measurements of the microtremor sites were deployed at nine different locations in the Eskişehir Graben, as shown in Fig. 6. The nine sites were located on alluvial units 2, 3, 4, 6, 7, 9, 11, 12 and 13. The investigation utilized a Guralp CMG-6TD-series wireless recording system, with four sensors used in each array (Fig. 7a). Data were recorded using 24-bit analogue-to-digital (A/D) wireless recorders with a 100-sps sampling interval, with three accelerometers aligned at the edge of the equilateral triangle and one sensor at the centre of the circle for SPAC applications, to provide phase velocities (Fig. 7b). These measurements were repeated for three different radii ($r_1 = 10$, $r_1 = 30$, $r_1 = 90$ m).

During the measurements, recordings were taken with openings varying between 10 and 90 m, in the form of three equilateral triangles. For the triangle configuration at MAM location 7, in calculating the dispersion curves from data obtained from the microtremor array records, the principles set out in the (Bard & SESAME Team 2005) project were taken into consideration. The Rayleigh wave dispersion curve inversion was performed using the Geopsy software package (http://www.geopsy.org; Wathelet *et al*. 2008). The correlation between the SPAC coefficients obtained from the observational values and the theoretical Bessel function were investigated (Fig. 8), and values belonging to the correlated frequency interval were used in the calculation of the dispersion curve. The SPAC results were displayed using 'spac2disp', and the relationship between the autocorrelation coefficients and phase velocities for the different arrays ($r = 10$, 30 and 90 m) were investigated. For the arrays with radii of 10, 30 and 90 m, correlation results were obtained for the frequency ranges of 2–6, 1.5–4 and 1–2 Hz, respectively.

The data inversion was performed using the Dinver module, which uses the Natural Neighbourhood Algorithm (Sambridge 1999a,b), which was later modified by (Wathelet 2008). We present

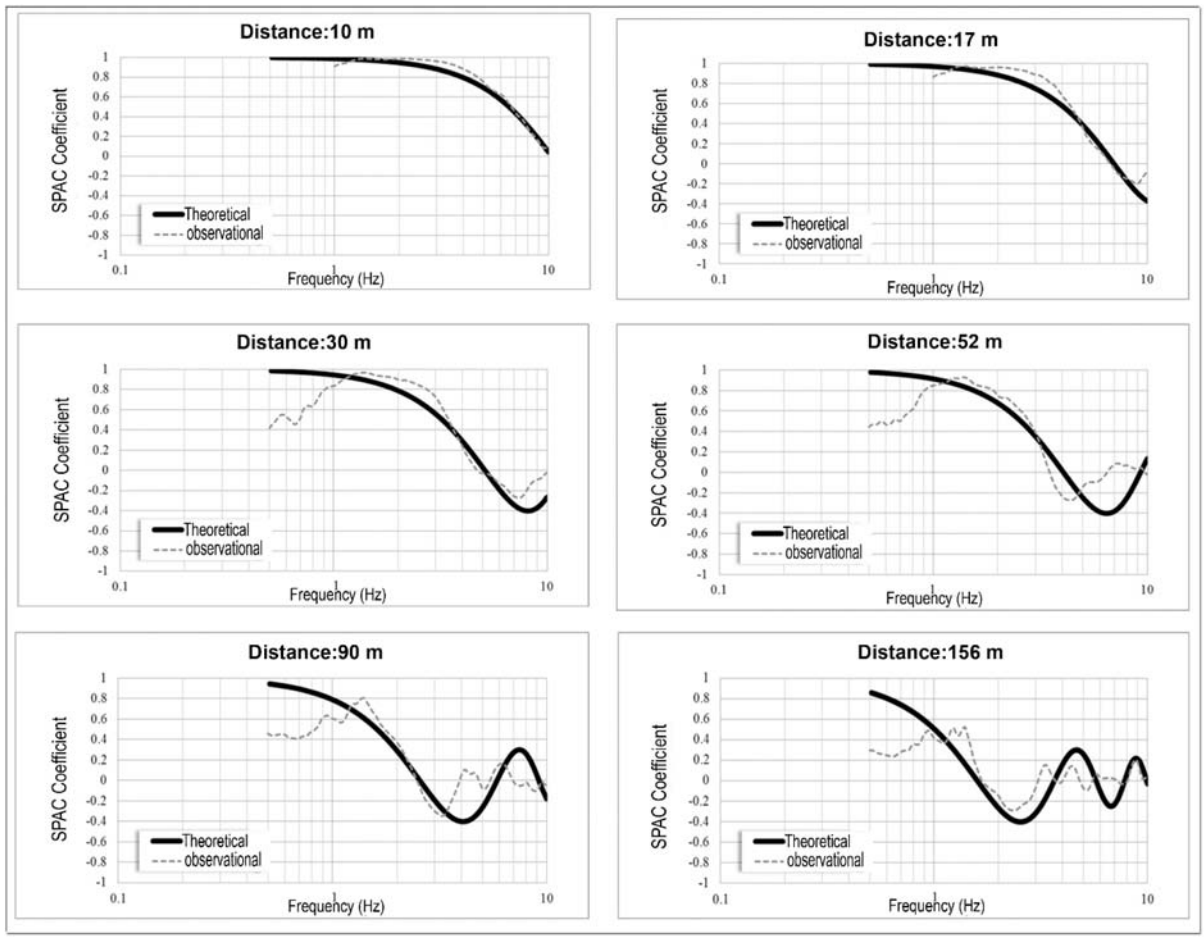

Figure 8. An example of the investigation of the correlation between SPAC coefficients and theoretical Bessel functions for MAM measurement point 2.

the data processing steps for the determination of the dispersion curve and the inversion steps for determining the *S*-wave velocity profile in Fig. 9. Initially, the layer thickness was held constant during the inversion process, and the most accurate solution was sought by modifying the *S*-wave velocities and layer thickness parameters. As a result, the shear wave velocity profiles were obtained using the iterative linear inversion process (Park *et al*. 1999). In this approach, the measured dispersion curve is first transformed from the $c(f)$ to the $c(\lambda)$ domain simply by dividing the phase velocities by their corresponding frequencies. Then, λ is divided by two to obtain the initial *S*-wave profile $V_s(h)$ as a function of depth. Finally, $V_s(h)$ is converted to a layered initial model. MAM location 2 is a site located on the northwest edge of the Eskişehir Basin, surrounded by hills (Fig. 6). At this site, we observed only fundamental-mode Rayleigh wave dispersions. The observed dispersion data are indicated by black dots with their corresponding standard deviations in Fig. 9(c). The observed dispersion data are shown by black dots with their corresponding standard deviations in Fig. 9(c). The inversion of the dispersion curves is non-unique, so Fig. 9(b) shows the ensemble of inverted shear wave profiles that explain in a similar way the observed phase velocities. The dispersion curve, which was determined using the frequency wave number method, is plotted in grey in Fig. 9(c) for comparison. The minimum misfit found was 0.12, and the averages and standard deviations (vertical bars) of the apparent dispersion curves from the arrays are shown in Fig. 9(b). Information on the sites and the parameter values obtained in this study are given in Table 1. The same processing steps were carried out for all nine sites.

MAM measurements from nine of the 13 points could be interpreted; the other records could not be assessed because they were affected by ambient noise. The MAM measurements points that were used were those numbered 2, 3, 4, 6, 7, 9, 11, 12 and 13. The dispersion curves obtained from the microtremor array measurements from the nine different points are shown in Fig. 10. The sites of the microtremor array measurements were distributed among the same surface geological units at the city centre. The dispersion curves showed wide frequency ranges in the phase velocities (0.5–10 Hz). The dispersion curves varied with the thicknesses of the young sediments, and the curves can be categorized as belonging to three sites (Fig. 10). At Site 1, among SP04, SP12 and SP02, the highest velocity was approximately 800–1100 m s^{-1}, although the velocity fell to 300 m s^{-1} at higher frequencies at these sites. At Site 2, the phase velocities of SP03, SP07, SP09 and SP13 were between 250–700 m s^{-1} in the frequency ranges below 10 Hz. At Site 3, the dispersion curves of SP11 and SP06 were very discrete with respect to the other sites, with the lowest calculated velocity (approximately 300 m s^{-1}).

The dispersion curve obtained from the depth–V_s variation derived using the SPAC method and Rayleigh analysis is shown in Fig. 11. The bedrock depth was found to be 255 m from SPAC data number 2, 140 m from SPAC data number 4, 395 m from SPAC data number 9 and 500 m from SPAC data number 13. In the

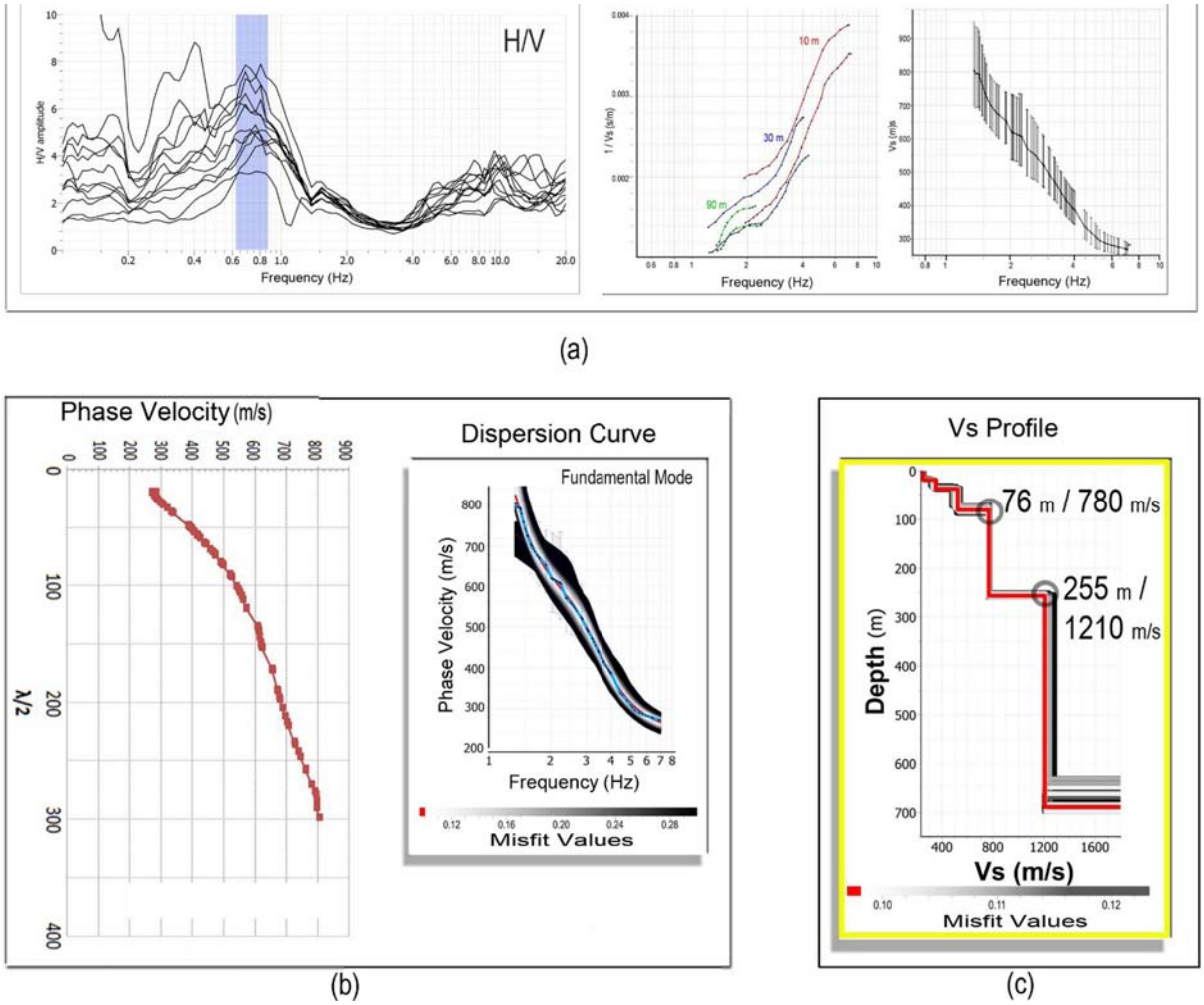

Figure 9. Determination of the dispersion curve for site MAM location 2. (a) The HVSR curves for the MAM location and the combined dispersion curve (black) from the rings '10, 30 and 90 m'. The two curves corresponding to each colour correspond to the upper and lower limits for fundamental-mode Rayleigh wave dispersions. (b) The wavelength–phase velocity relationship from $c(f)$ to $c(\lambda)$. The corresponding dispersion curves are shown in grey scale, and the combined dispersion curve obtained from the SPAC is shown in blue. Derived dispersion curves for misfit lower than 0.28, corresponding to extracted models. (c) The V_s profile from the dispersion curve. The red line in the figure represents the velocity profile of the true model. Information on the sites and the parameters obtained in this study are given in Table 1. The AV_{s30} was calculated from the joint inversion of the dispersion curve and H/V, as described in Section 3.2.

Table 1. Station code.

No	Data	Lat. (°N)	Long. (°N)	Elev. (m)	Geology	AV_{s30} (m s^{-1})	NEHRP site class	Ave. Ampl. (0.2–10 Hz)	f_r (Hz)
1	MAM SPAC02	39.81725	30.42447	823	New Alluvium	261	D	5.0	0.67
2	MAM SPAC03	39.79755	30.43946	813	New Alluvium	354	D	5.8	0.38
3	MAM SPAC04	39.76850	30.46354	793	New Alluvium	353	D	6.0	1.20
4	MAM SPAC06	39.82032	30.52842	787	New Alluvium	135	E	7.1	0.46
5	MAM SPAC07	39.78832	30.50398	796	New Alluvium	250	D	3.7	0.54
6	MAM SPAC09	39.83773	30.56839	785	New Alluvium	204	D	4.8	0.47
7	MAM SPAC11	39.77945	30.54756	787	New Alluvium	175	E	8.9	0.87
8	MAM SPAC12	39.75474	30.58052	792	New Alluvium	311	D	4.1	1.25
9	MAM SPAC13	39.80706	30.63067	781	New Alluvium	203	D	5.9	0.38

course of examining the V_s depth profiles of the Eskişehir Basin in the NE–SW direction, the velocity variation along the S3–S4 transverse section shown in Fig. 6 was investigated because it was believed that it might reflect the overall velocity profile of the entire basin (Fig. 11b). Based on the SPAC solutions, as well as previous geophysical, geological and geotechnical studies carried out in the region (Başbakanlik-PUB-MEER 2006), it was concluded that on the transverse velocity section obtained, the bedrock geometry may have a half-graben structure. The upper sediment–bedrock boundary was defined as the depth at which the V_s velocity reaches 1200 m s^{-1}. It was observed that the upper sediment thickness was approximately 400 m on the NW border of the Eskişehir Basin.

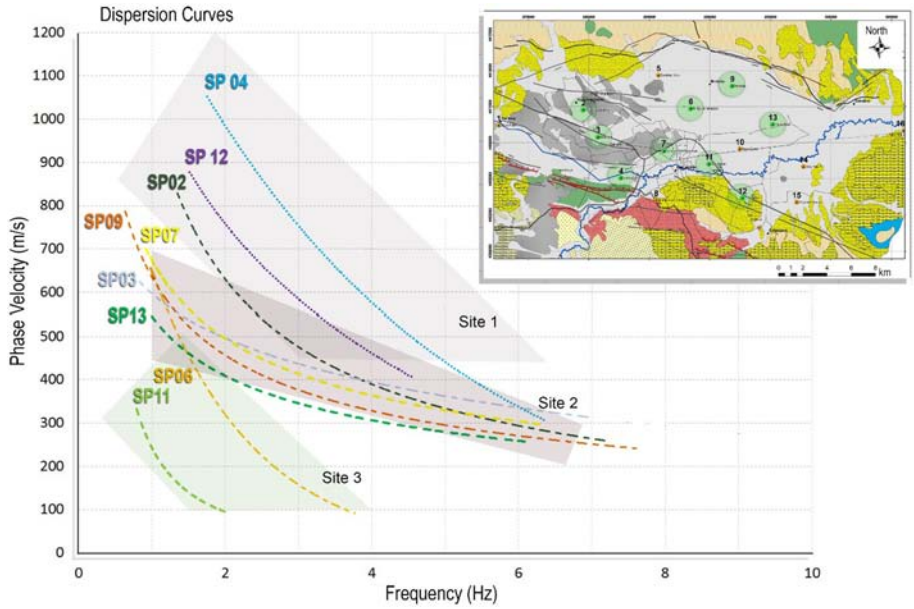

Figure 10. Dispersion curves for MAM locations.

The *S*-wave velocity obtained from the SPAC method was found to range between 1020 and 1240 m s^{-1} in the bedrock, according to the generated models.

The profiles in Figs 6 and 11 indicate the presence of nearly vertical faults at sites SPAC 4 and SPAC 7. Another important feature shown Fig. 11 is a thin layer with a low *S*-wave velocity (representing the lower limit of the range, 160 m s^{-1}) covering the horizontal distance between SPAC 7 and SPAC 9.

3.2 Validation of the SPAC results with joint inversion

A joint inversion of the phase velocity and H/V ratio curves, both obtained from seismic noise recordings, permits the retrieval of the shear wave velocity structure of the local sedimentary cover (Parolai *et al*. 2005). The possibility of explaining the dataset using a simpler model representing two overlying layers was investigated. Each layer was characterized by its thickness H, density ρ, *P*-wave velocity V_p, and *S*-wave velocity V_s (Table 2). The *S*-wave velocity and thickness were varied for each layer.

In this study, the V_s profiles were obtained using the MAM-SPAC method and single-station microtremor measurements (inverted). The dispersion curve observed for the frequency wavenumber method is plotted in grey in Fig. 12 for comparison. The minimum misfit found was 0.12. The averages and standard deviations (vertical bars) of the apparent dispersion curves from the arrays are shown in Fig. 12. The HVSR curves obtained from the single-station microtremor measurement (observed) and computed from the theoretical model (inverted) are shown for MAM-SPAC locations 2 and 13 in Fig. 12. The H/V ratio curve obtained using a transfer function (GEOPSY-gpell.exe) and the V_s–depth variation are shown for MAM-SPAC measurements points 2 and 13 in Fig. 12. In both cases, at MAM location 2, the velocity was found to be more than 780 m s^{-1}, and it was observed that the engineering bedrock starts approximately 80 m from the surface, whereas the seismological bedrock, at which the velocity exceeds 1200 m s^{-1}, starts at a depth of approximately 250 m. In both cases, at MAM location 13, the velocity was found to be more than 750 m s^{-1}, and it was observed that the engineering bedrock starts approximately 170 m from the surface, whereas the seismological bedrock, at which the velocity exceeds 1150 m s^{-1}, starts at a depth of approximately 500 m.

The *S*-wave velocity in the bedrock of the generated models ranges between 800 and 1200 m s^{-1} and between 800 and 1100 m s^{-1} for MAM locations 2 and 13, respectively (Fig. 12).

3.3 Seismic reflection studies in the Eskisehir Graben

Several seismic reflection surveys using a P-Gun have been carried out in the Eskişehir Basin, partially covering the new alluvium and the bedrock depths and sediment thicknesses, which have been observed at four different locations in the Eskişehir Basin (Fig. 6). The P-Gun fires 36 cartridges downwards simultaneously, generating *P*-waves, a 94-ton pick force, and a penetration depth of more than 1000 m. We adapted the walk-away multichannel seismic reflection data acquisition technique for P-Gun surveys (Fig. 13), which is a layout technique in which the receivers remain stationary while the shots move. On certain lines, the distance between receivers was 10 m, with shootings made every 25 m; on other lines, these distances were 5 m and 15 m, respectively.

An average of 25 shots were made in the P-Gun surveys and provided a horizontal seismic section width of approximately 480 m and a penetration depth of approximately 1500 m. The shot interval was 10 m, the group interval (one geophone per group, 96 geophones in total) was 10 m, the near offset was 10 m, the far offset was 960 m, and the CDP interval was 5 meters. The researchers selected 0.5 ms as the sampling interval and 2 s as the recording time for use with the P-Gun. No digital or analogue filters were used during recording, and all filtering was left to the seismic processing stage. The seismic data were processed using the licensed WGeosoft's Visual_SUNT v11 software package.

Seismic data processing steps:

(1) Geometry definition.
(2) Band-pass filters: 1, 5, 90 and 100 Hz.
(3) Automated gain control time window: 500 ms.
(4) Static correction.
(5) First-breaks mute.
(6) Ground-roll mute.

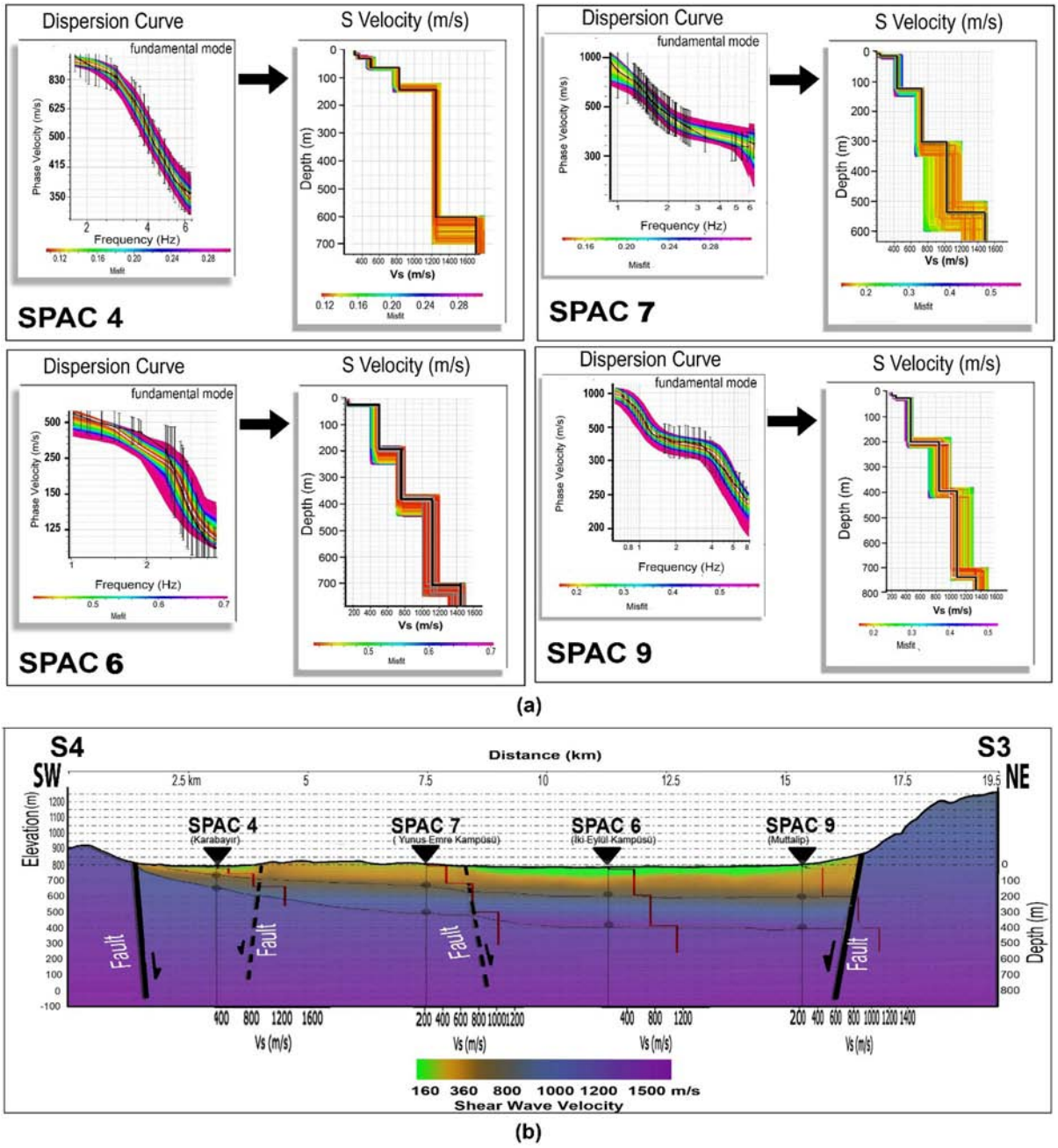

Figure 11. (a) Observational dispersion curve and V_s depth profile for MAM-SPAC measurement points 4, 7, 6 and 9. (b) The sediment–bedrock depth cross-section of the Eskişehir Basin, based on the selected V_s profiles along the S3–S4 profile. The image was generated by gridding the four selected V_s profiles (red lines). The bold black line on the image represents the faults, and the thin black line represents the sediment–bedrock interface.

Table 2. Inversion parameters.

No	Site	Depth range (m)	Density (g cm^{-3})	V_p range (m s^{-1})	V_s range (m s^{-1})
1	MAM SPAC 02	35–100	1.6–2.0	550–1100	300–750
		100–300	2.2	2500	1200
		>300	2.4	4500	2500
2	MAM SPAC13	15–160	1.5–1.9	450–900	250–650
		160–500	2.0	2500	1200
		>500	2.5	4500	2500

(7) CDP sort (Major key: CDP, Minor key: Signed offset).
(8) Velocity analysis (at six CDP stations and velocities of 500 to 4000 m s^{-1}) and stack.
(9) Lateral smoothing, with weighting factors of 0.25, 0.5, 1, 0.5 and 0.25.
(10) Conversion from time to depth.
(11) Creation of image file of the seismic sections.

The bedrock is an almost horizontal and continuous seismic horizon that produces a rather strong reflection. Under the bedrock, the seismic texture is irregular.

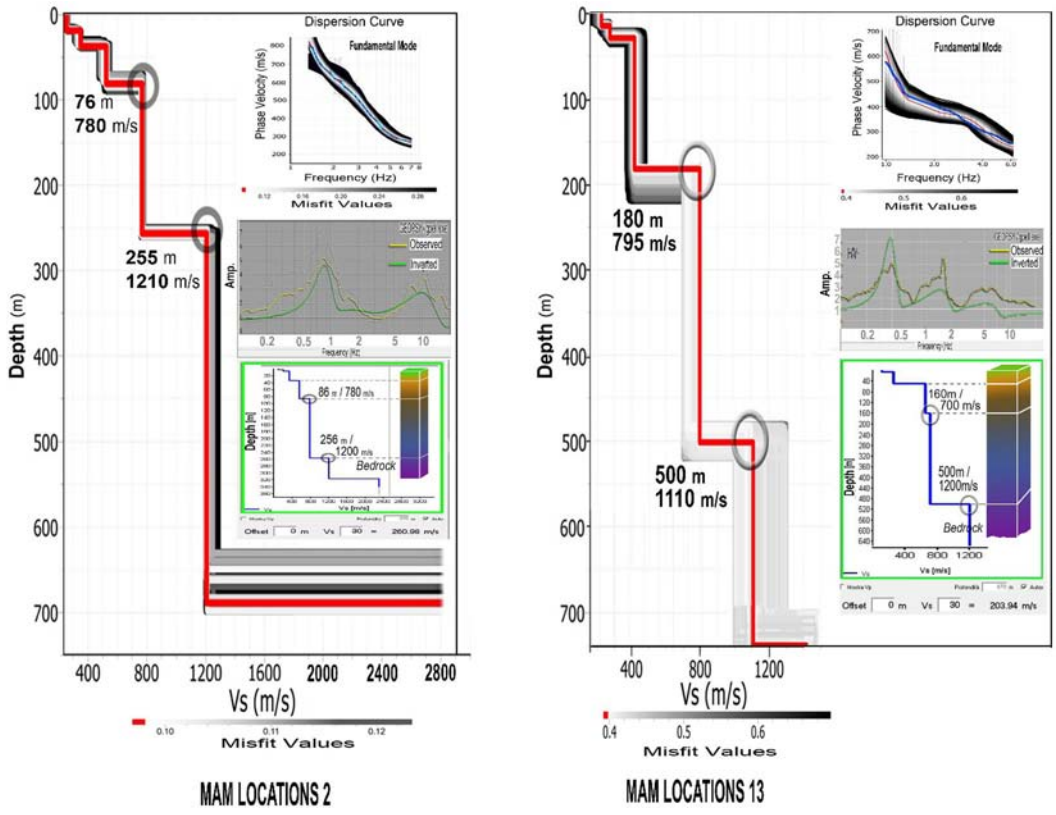

Figure 12. Combined inversion (dispersion + HVSR) results for MAM locations 2 and 13, with the corresponding dispersion curves (grey scale) and the combined dispersion curve obtained from the SPAC (blue). Derived dispersion curves for misfits lower than 0.28 and 0.6 corresponding to the extracted models. The V_S profile from the dispersion curve. The red line in the figure represents the velocity profile of the true model. The combined HVSR curve obtained from a single-station microtremor measurement (observed), computed from theoretical model (inverted). The V_S profile from the inverted model + HVSR

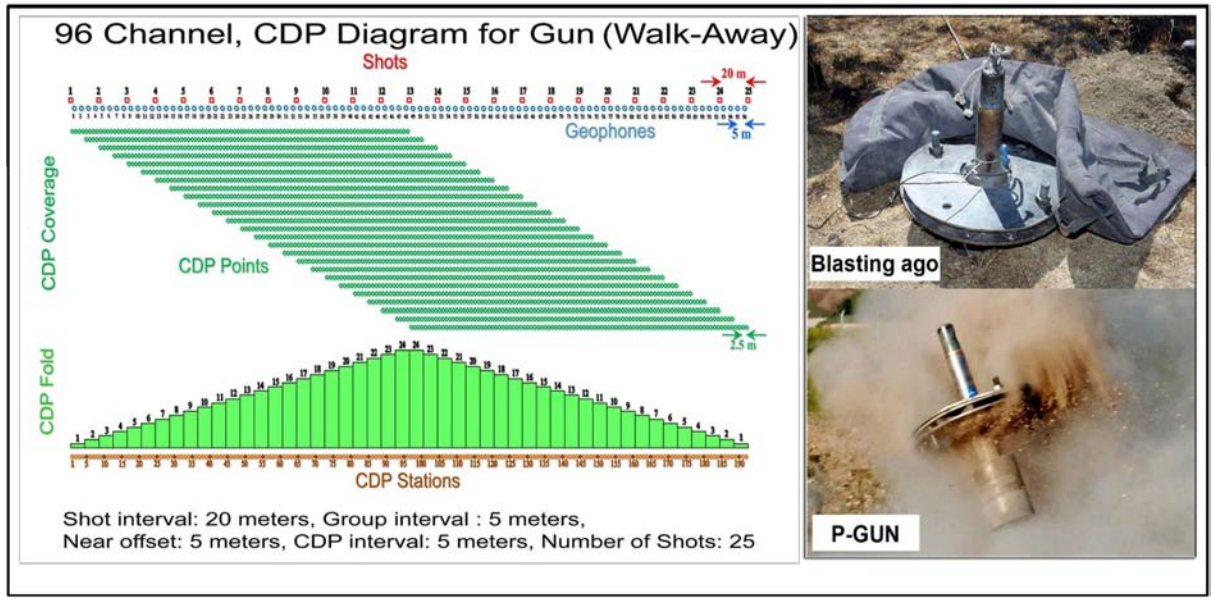

Figure 13. CDP diagram for the walk-away technique, shooting line S2 (480 m), 36-barrel P-Gun (seismic source) and blasting of cartridges and seismic recorder (Geometrics 24-Channel Geode Modules) located in the middle of the 48-channel (14-Hz P-Geophones) walk-away technique range.

In this figure, the red line represents the bedrock depth (Fig. 14), and in the seismic sections, the sedimentary thickness was found to be at a depth of more than 600 m. The bedrock depths in the seismic section that generated the seismic reflection data were 250, 120, 400 and 500 m for sections S-2, S-4, S-9 and S-13, respectively (Fig. 14). The bedrock depth obtained from the seismic reflection data were compatible with the joint inversion of the phase velocity and H/V ratio curves obtained during the seismic noise recordings.

In the seismic sections obtained from S-2, S-4 and S-9, the blue lines are thought to correspond to the oldest formation (basement

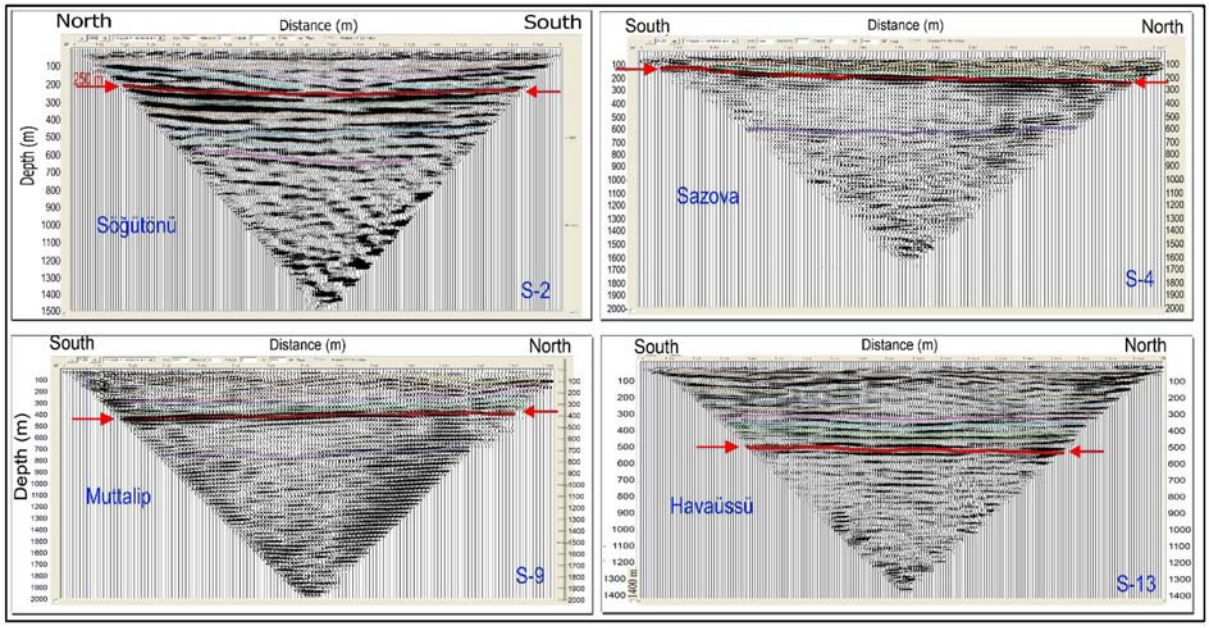

Figure 14. Interpreted seismic reflection data from S-2, S-4, S-9 and S-13. For locations, see Fig. 15. The red lines indicate the bedrock depth. V_s = 800–1300 m s^{-1}.

rock) and appear as tectonic units comprising Triassic-aged Eskisehir Metamorphics in the study area. These basement rock units are covered by varying thicknesses of sedimentary material with stiff overlying low-shear-wave-velocity units, resulting in a sharp velocity contrast. The red lines in the seismic section result from the large impedance contrast between the soft sediments and the bedrock.

4 RELATIONSHIP BETWEEN FUNDAMENTAL FREQUENCY AND SEDIMENTARY COVER THICKNESS

A number of studies (Ibs-von Seht & Wohlenberg 1999; Özalaybey *et al*. 2011; Tün 2013) have shown that the resonance frequency obtained from microtremor measurements can be used to map the thickness of sediments. In this study, borehole data (from three sites), MAM data (from nine sites), reflection surveys (from eight sites) and shallow drilling data (from 10 sites) (see Fig. 6) were used to calculate sediment thicknesses. The relationship between the top sediment thickness and the dominant frequency value shown in Table 2 was assessed, and an equation was developed to describe the relationship between the Eskişehir Basin bedrock depth and f_r (Fig. 15a). A comparison of the published relationships (Fig. 15b) shows a similarity curve obtained from $h = af_r^{-b}$, for which the values of the parameters (a and b) of the inverse power relationship are established (Ibs-von Seht & Wohlenberg 1999) using a fitting technique.

For the regression, the locations at which HVSR curves with well-defined spectral peaks were obtained were selected, and the f_r values obtained for these locations were used. Other sources (Ölmez *et al*. 1986; Azdiken & Çatalyürekli 2001; Sevinçli & Çatalyürekli 2001; Başbakanlik-PUB-MEER 2006; Tün *et al*. 2010) were used for additional deep drilling data, shallow drilling data, and other seismic reflection section data, beyond those obtained for this study. The dominant frequency–bedrock depth relationship obtained in this way for the Eskişehir Basin is given in eq. (3). The relationship between the dominant frequency and the bedrock depth is a simplified representation and does not consider the complexities of the shallow subsurface structure.

$$h = 136 f_r^{-1.36} \quad (3)$$

It is worth noting that the regression coefficients *a* and *b* in eq. (3) are similar. The bedrock depth spatial variations map, drawn using eq. (3) for the f_r values obtained from 318 different points within the Eskişehir Basin, is given in Fig. 16. As the figure shows, the maximum bedrock depth is 1000 m in the northeastern portion of the study area. The maximum depth was determined for an area 100 m south and 600–1000 m northeast of the study area, which indicates that the Eskişehir Basin has a locally rather thin sedimentary cover, with stiff overlying low-shear-wave-velocity units, resulting in a sharp velocity contrast.

Within the boundaries of the Eskişehir Basin, the spatial variation of the bedrock thickness in the area bordered by the elevations in the north and south (Fig. 16) shows that the bedrock thickness is 700 m in the northern portion of the basin and decreases to 100 m to the south. This structure, which dominates the entire the basin, has the characteristics of a half-graben. A section of the basin was taken along a NE–SW diagonal to examine the half-graben structure and the compatibility of the graben geometry, with the existing faults. Fig. 17 shows the sediment–bedrock thickness relationship calculated from the HVSR curve f_r values along the A–A′ profile (see location in Fig. 1). The A–A′ cross section with H/V variations at sites 33, L13, J15, I16, G16, G18, E18, D18, B18, A18, 86, 85 and 83 is shown in Fig. 17.

4.1 Verification of bedrock depth using the borehole data for the Eskisehir Graben

The borehole log coded BH AÜ for a location close to the site of HVSR recording I7, J6 (latitude 39.764°, longitude 30.485°), and in the southwestern part of the Eskisehir Basin (Fig. 6), was planned to a depth of 100 m, and drilling was carried out to a depth of 90 m at a location at which it was expected that the bedrock could be reached. The results obtained are shown in Fig. 18. The borehole log

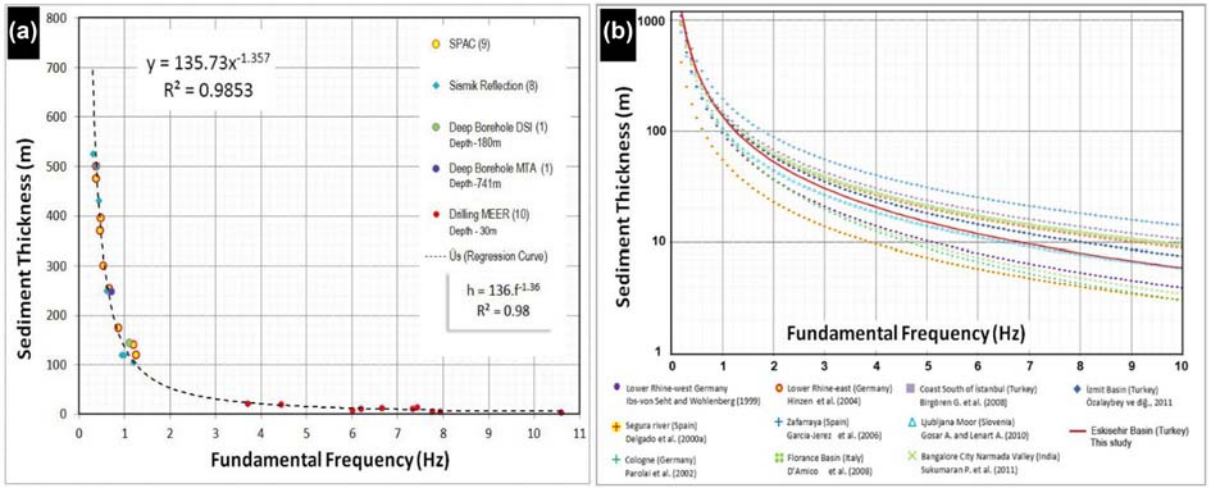

Figure 15. (a) Fundamental resonance frequencies versus sediment thickness, derived from SPAC, seismic reflection, deep boreholes and drilling in the Eskisehir Basin. The black dashed line represents the fit to the data points, according to eq. (3). (b) The frequency–thickness relationship curves for 10 sedimentary basins, from the literature and for the Eskisehir Valley.

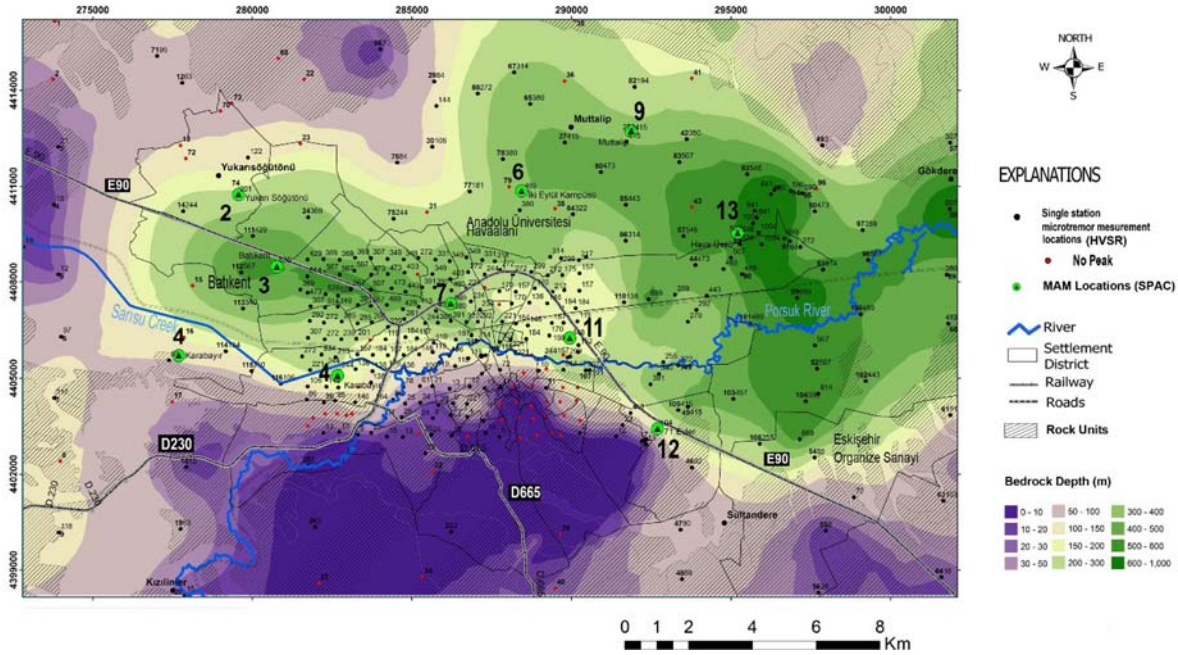

Figure 16. Bedrock depth map of the Eskişehir Basin generated using single-station microtremor records.

information shows that the first 2 m of material is topsoil, the material 2–6 m deep is Quaternary-age New Alluvium, and the material from 6–18 m deep is Old Alluvium. The Old Alluvium layer continues with a clay–silt unit (18–39 m) of a light cream-grey whitish colour. In this unit, sandstone bands and gravel of various sizes were observed in patches. Below this level (39–76 m), on the other hand, is a unit containing alternating layers of clay, sand, silt, schist, and sandstone (Tertiary age), which starts with a light pinkish colour, becomes dark brown, and then turns back to a light pinkish colour. Between 79 and 90 m, there is a partly cracked yellowish-greenish ophiolite unit (Triassic age) that has undergone alterations. The Eskisehir Basin is covered with Tertiary and Quaternary sediments overlaying Triassic bedrock. The upper sediments consist of lower Eocene to Pliocene conglomerates, basalt, tuff and sandstone covering Triassic ophiolite, marble and green schist. At the top, alluvial sediments were deposited during the Pleistocene. The ophiolite unit is described as the bedrock in the study area. According to eq. (3), h calculated as $136\ (1.5)^{-1.36} = 78$ m. It is quite compatible with the results obtained from the borehole data.

5 DISCUSSION

The f_r map illustrates variations that are seemingly consistent with the surface geology and spatial extent of the basins present in the Eskişehir Graben. The sites located in the northern part of the study area have fundamental frequencies in a low frequency range (0.2–1 Hz), as shown in Fig. 5, while the sites located in the southern part have fundamental frequencies in the range of 2.0–20 Hz. The central area of the basin, which has a Quaternary geology, has the lowest fundamental resonance frequencies (0.2–0.5 Hz, indicated in dark green in Fig. 5). The f_r values increase smoothly from these values over short distances (0.5–1 Hz, indicated in light green) and

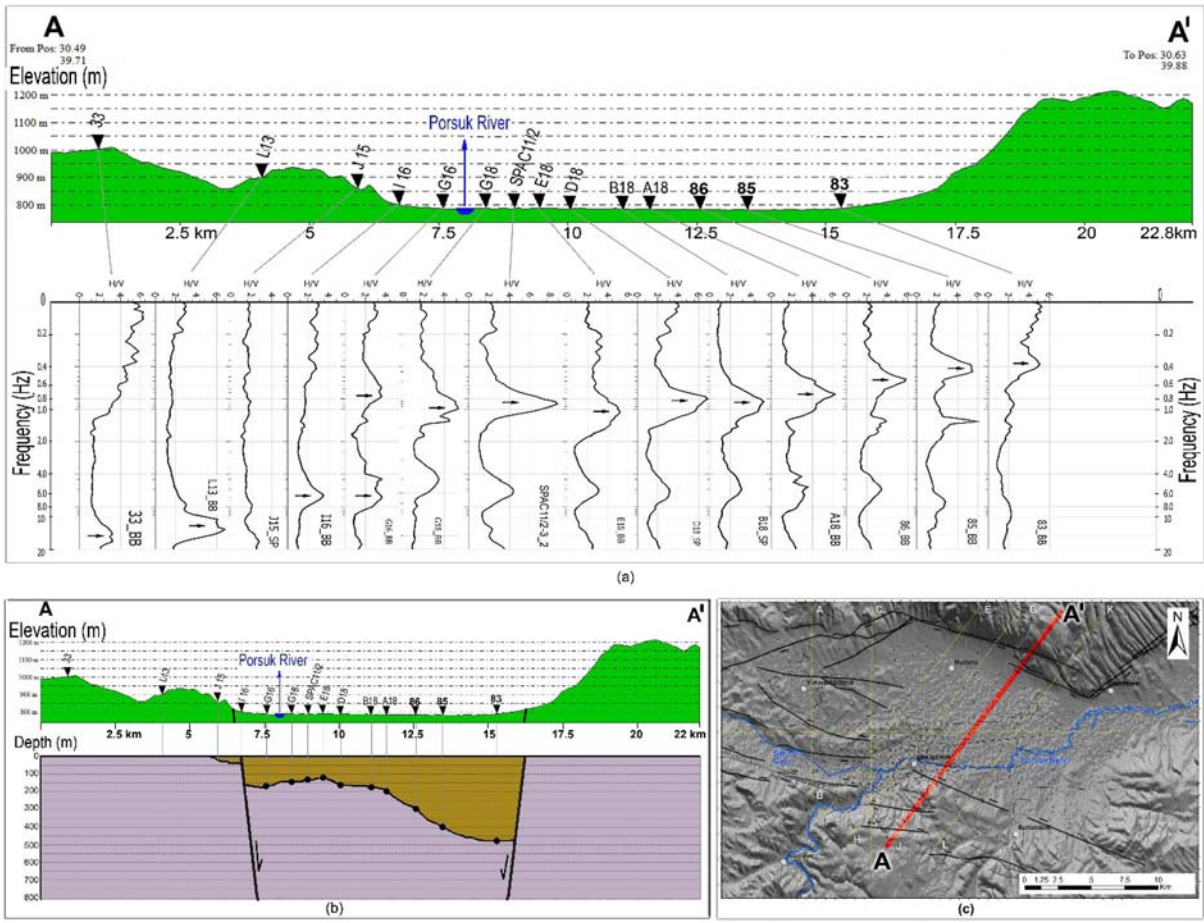

Figure 17. The sediment–bedrock depth cross-section of the Eskişehir Basin, based on the selected calculation from the HVSR curves along the south–north profile A–A′, is shown in Fig. 1(b). (a) The locations of the selected HVSR curves (black inverted triangles) are projected onto the topography shown at the top. (b) The image at the bottom shows the bedrock depth along the A–A′ profile. (c) The A–A′ cross-section on the topographic map.

change sharply to values ranging between 1 and 5 Hz (yellow- and orange-coloured sections in Fig. 5 near the basin margins with thin quaternary cover. It is apparent that the variations in the f_r values, which reflect the varying thicknesses of the sediment, result in the greatest contrast in impedance at the interface of the bedrock in the study area. An interpretation of H/V curves (Figs 3 and 4) indicates that the secondary peak in the medium- to high-frequency range (4–8 Hz) may be related to the upper-level soil layer, which is composed of Quaternary sediments from the Eskişehir Plain and clasts accumulated by the Porsuk River and Sarisu Creek.

In Fig. 17, we present an NE–SW cross-section taken at the centre of the basin to illustrate the shape of the basin in 2-D. The section shows that the basin boundary extends to a depth of 200 m on the plane until it reaches the centre of the Eskisehir Basin and then extends in depth with a sharp dip at an angle of 45° towards Muttalip Peneplain from the Odunpazari side, reaching a depth of 1000 m. The shape, which is that of the half-graben, is consistent with the fault segment within the basin boundaries.

Cross-section A–A′, indicating the H/V variations at sites 33, L13, J15, I16, G16, G18, E18, D18, B18, A18, 86, 85 and 83, is shown in Fig. 17. It is interesting to note that the H/V at sites 33 and L13 (south and north of the Cukurhisar–Sultandere fault segment, respectively, located in the southern part of the study area shown in Fig. 1 exhibit one peak at high frequencies. Both sites are located on limestone (Porsuk Formation–Upper Miocene–Tertiary). In addition, a similar HVSR pattern can be observed at sites L8 and L18, located close to site L13, as shown in Fig. 3. Close to sites L13 and L18, there is a fault that cuts across Triassic rocks (Figs 1, 4 and 6). As Fig. 17(c) shows, the southern part of section A–A′ (sites close to A) cuts across three segments of faults located at a site featuring metamorphic rocks. It can thus be speculated that this part of the study area is densely fractured. The fact that the H/V at these sites exhibits one peak at high frequencies may be related to the presence of a fractured limestone bedrock (Parker & Hawman 2012). To the south of the basin, SP04 shows that the shear wave velocities at depths of between 50 and 100 m, for example, are high (e.g. approximately 800 m s^{-1} at 60 m). At sites SP09 and SP13, located in the north of the basin, the shear wave velocities at depths of between 50–100 m are lower (see Figs 11 and 12).

The remainder of the sites G16–85 (section A–A′, Fig. 1) exhibit two amplified peaks, with the fundamental H/V peak in the low frequencies and a second peak in the frequency range of 4–8 Hz. The surface geology of those sites is characterized by Quaternary sediment (recent alluvium on top, Fig. 1), and the seismic reflection method revealed a bedrock depth of 400–600 (Fig. 14). Previous studies have revealed the existence of fault segments (Figs 1 and 6) to the west of this section, where the amplified peak in the low-frequency range is related to locally soft or thick sediments, and the second peak, in the medium- to high-frequency range (4–8 Hz), is possibly related to the shallow subsurface of the upper-level soil layer, which is composed of Quaternary sediments. Locally, there are sites presenting broad H/V peaks at medium to high frequencies,

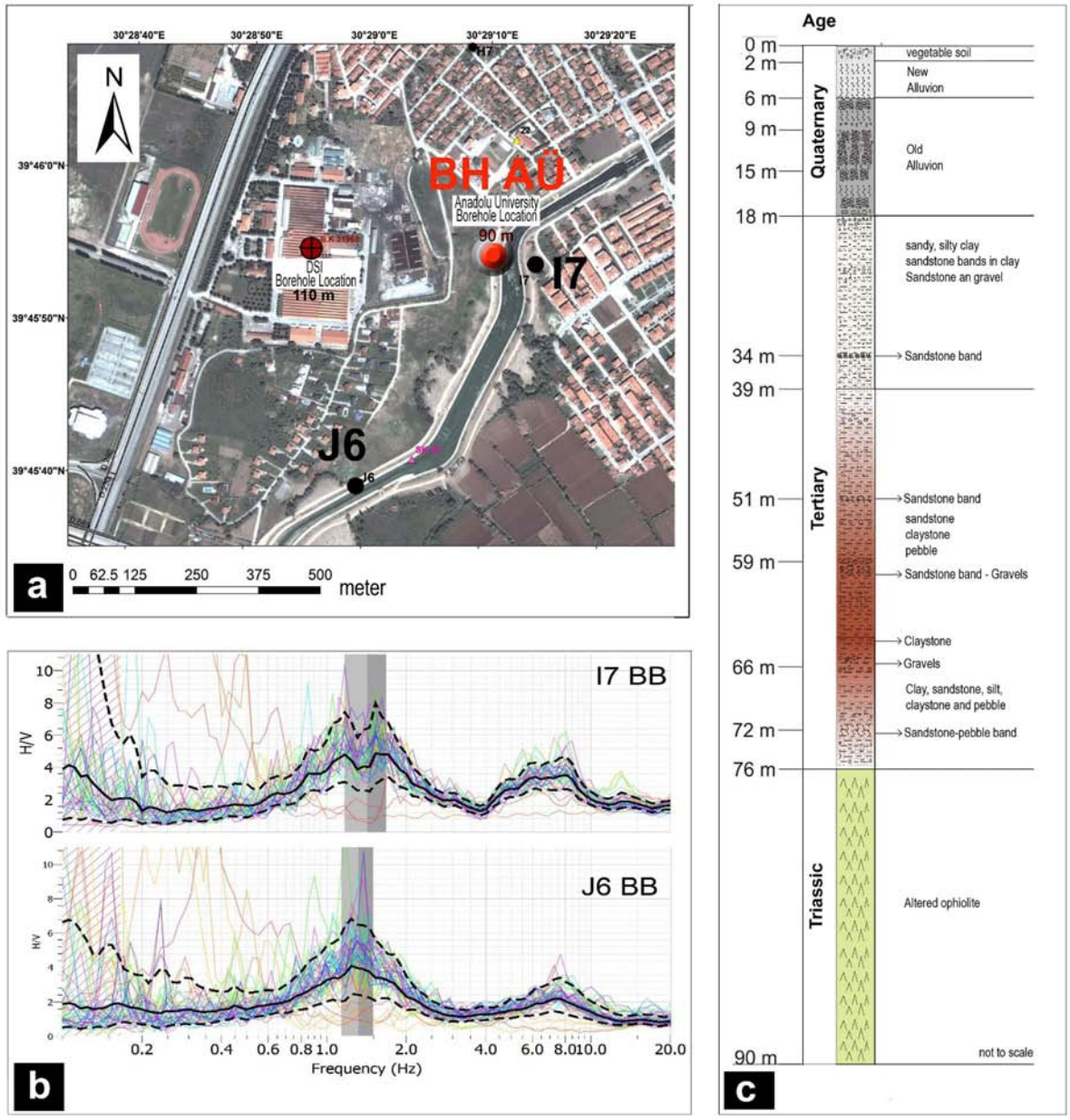

Figure 18. Anadolu University drilling well logging. For location, see Fig. 6: (a) Coded 'BH AÜ'. Drilling location (b) HVSR curves for I7 and J6 (c) borehole log.

which may be related to the complex seismic wave field of the shallow structure.

At site 83 (east of Muttalip), the one peak at low frequencies is related to the soft Quaternary or thick Quaternary deposits overlaying the metamorphic rocks. In the vicinity of site 83, the bedrock is 400–600 m deep (Fig. 17), and the surface geology is characterized by Quaternary deposits (Fig. 1). As described in Section 3.3, the seismic reflection revealed by P-Gun surveys identified thick sedimentary deposits at a depth of approximately 500 m (sites S-9, Muttalip, and S-13). In addition, the bedrock depth close to site 83, as derived from SP09 (Fig. 11), was found to be 395 m. Alluvial fan and fluvial deposits have been reported at those sites north of the Basin by Ocakoğlu (2007). A shallow layer with a low *S*-wave velocity at a horizontal distance of 7.5 km between SP07 to SP09 is shown in Fig. 11(b). The literature suggests that to the north of MAM measurement site no. 7 (see Figs 6 and 11), there is a normal fault inclined towards the NE, while in the south, there is a normal fault inclined towards the SW (Ocakoğlu 2007). These faults may have worked together to raise Pliocene deposits to higher levels than the Quaternary deposits in the central sections of the plain.

Site E2 (Fig. 4), where the surface geology is characterized by old alluvium Quaternary deposits (Fig. 1), presents only an amplified peak at low frequencies. Moreover, at site E2, the basement depth is approximately 500 m (Fig. 17), meaning that for site E2, the one amplified peak at low frequencies may be related to thick sedimentary deposits.

The dispersion curves obtained using the SPAC method are shown in Fig. 10. Frequencies in the range of 4–8 Hz are important in engineering terms because they have the potential to be correlated with the distribution of damage in the case of an earthquake event (Navarro *et al*. 2008). Furthermore, SP06 and SP11 presented the lowest phase–velocity values, ranging from 100–350 m s^{-1} for frequencies of 0.2–2 Hz. A more important feature is the existence of a soft shallow layer at the SP11 location.

6 CONCLUSIONS

We have shown that the impedance contrast at the sediment–bedrock interface has a strong influence on the shape of the H/V ratio curve around the fundamental frequency. This allowed us to determine the geometry of the bedrock depth in the study area. The bedrock structure of the Eskişehir Basin was studied on the basis of H/V and SPAC analyses, seismic reflection and borehole data. The shear wave velocity and thickness of the sedimentary cover were determined from the phase–velocity dispersion curve and f_r of the H/V ratio curve, respectively. The main results of the study are as follows: (1) the depth of bedrock reaches a maximum of 1000 m (Fig. 16); (2) the geometry of the Eskişehir Basin is a half-graben (Fig. 17); (3) the phase–velocity values provided dispersion curves (Fig. 10) in the range of 100–1100 m s^{-1} for frequencies of 0.2–10 Hz; and (4) the amplified peak in the low-frequency range is related to locally soft or thick sediments, while the second peak, in the medium- to high-frequency range (4–8 Hz), may be related to the upper level soil layer, which is composed of Quaternary sediments.

The city of Eskişehir is located 5–7 km from the northern edge of the half-graben. Strong ground motions, which have caused severe damage to the city, are considered to have resulted from amplification due to the geometry of the bedrock depth. The results of an investigation of the 3-D geometry of the bedrock depth can serve as basic information for use in microzoning of an urban area in a sedimentary basin.

The basin structure, the lower-boundary bedrock geometry, and the resonance effects resulting from layer thicknesses on top of the bedrock are factors that are known to have the potential to cause soil amplification. In this regard, the identification of the bedrock surface boundary geometry along the lower basin boundary is of utmost importance when attempting to estimate the resonance and focusing effects in a future earthquake. Data on the bedrock depth geometry and the velocity profile are also needed when carrying out a regional seismic risk analysis and seismic hazard calculations, and so are of great importance in understanding the seismicity of a location.

ACKNOWLEDGEMENTS

This research was supported by the Anadolu University Research Fund under Project Numbers 080240 and 1401F026. We would like to thank Prof Berkan Ecevitoğlu (Anadolu University Eskişehir) for sharing with us his experience related to seismic interpretation; Prof Gürol Seyitoğlu (Ankara University) for sharing his knowledge of the region; Assist. Prof Savaş Karabulut (Istanbul University) for his experience in microtremor recordings; and Doğan Kalafat (Boğazici University, Kandilli Observatory and Earthquake Research Institute), who provided details of the 2003 and 2013 events. We are also deeply indebted to Prof Naci Gündogan, and the former and current presidents of Anadolu University for their invaluable support in this study.

REFERENCES

AFAD, 1996. *Earthquake Zoning Map of Turkey*, Republic of Turkey Prime Ministry Disaster & Emergency Management Authority.

Aki, K., 1957. Space and time spectra of stationary stochastic waves, with special reference to microtremors, *Bull. Earthq. Res. Inst. Univ. Tokio,* **35,** 415–456.

Aki, K., 1965. A note on the use of microseisms in determining the shallow structure of the Earth's crust, *Geophysics,* **30**(4), 665–666.

Altunel, E. & Barka, A., 1998. Neotectonic activity of Eskişehir fault zone between İnönü and Sultandere, *Geol. Bull. Turkey,* **41**(2), 41–52.

Asten, M., 1976. The use of microseisms in geophysical exploration, *PhD thesis,* Macquarie University.

Atakan, K., Bard, P.Y., Kind, F., Moreno, B., Roquette, P. & Tento, A., 2004. J-SESAME: a standardized software solution for the H/V spectral ratio technique, in *Proceedings of the 13th World Conference on Earthquake Engineering,* Vancouver, Canada, pp. 1–6.

Azdiken, S. & Çatalyürekli, E., 2001. General Directorate of State Hydraulic Works, Eskişehir Odunpazari Municipality Geophysics Resistivity Report.

Bard, P., 1998. Microtremor measurements: a tool for site effect estimation? in *Second International Symposium on the Effects of Surface Geology on Seismic Motion,* Vol. 3, pp. 1251–1279, eds Irikura, K., Kudo, K., Okada, H. & Sasatani, T., Balkema, Rotterdam.

Barka, A., Reilinger, R., Şaroğlu, F. & Şengör, C., 1995. The Isparta Angle: its importance in the neotectonics of the Eastern Mediterranean Region, in *Proceedings of the International Earth Sciences Colloqium on the Aegean Region,* vol. 1, pp. 3–17, eds Pişkin, O., Ergün, M., Savaşçin, M.Y. & Tarcan, G., 9–14 October 1995, Izmir-Golluk, Turkey.

Bard, P.Y. & SESAME Team, 2005. Guidelines for the implementation of the H/V spectral ratio technique on ambient vibrations-measurements, processing and interpretations, Site EffectS assessment using AMbient Excitations, European research Project, Project No. EVG1-CT-2000-00026.

Başbakanlik-PUB-MEER, T.C., 2006. *Microzonation and Hazard Vulnerability Studies for Disaster Mitigation: Eskisehir Preliminary Disaster Mitigation Plan,* Republic Of Turkey Prime Ministry Project Implementation Unit PIU.

Bonnefoy-Claudet, S. *et al.*, 2004. Simulation of seismic ambient noise: I. Results of H/V and array techniques on canonical models, in *Proceedings of the 13th World Conference on Earthquake Engineering,* Vancouver, Canada, 1–6 August.

Bonnefoy-Claudet, S., Cotton, F. & Bard, P.-Y., 2006. The nature of noise wavefield and its applications for site effects studies: a literature review, *Earth-Sci. Rev.,* **79**(3), 205–227.

Cornou, C., Kristek, J., Ohrnberger, M., Boore, D.M., Kudo, K. & Bard, P.Y., 2004. Simulation of seismic ambient vibrations: II. H/V and array techniques for real sites, in *Proceedings of the 13th World Conference on Earthquake Engineering,* Vancouver, Canada, August 2004, 1130 pp.

Delgado, J., Lopez Casado, C., Giner, J., Estevez, A., Cuenca, A. & Molina, S., 2000. Microtremors as a geophysical exploration tool: applications and limitations, *Pure appl. Geophys.,* **157**(9), 1445–1462.

Di Giulio, G., Cornou, C., Ohrnberger, M., Wathelet, M. & Rovelli, A., 2006. Deriving wavefield characteristics and shear-velocity profiles from two-dimensional small-aperture arrays analysis of ambient vibrations in a small-size alluvial basin, Colfiorito, Italy, *Bull. seism. Soc. Am.,* **96**(5), 1915–1933.

Dirik, K. & Erol, O., 2003. Tectonomorphologic evolution of Tuzgölü and surrounding area, central Anatolia-Turkey, *Turkish Association of Petroleum Geologists, Special Publications,* **5,** 27–46.

Emre, Ö., Duman, T.Y., Özalp, S., Elmacı, H., Olgun, Ş. & Şaroğlu, F., 2013. Active fault map of Turkey with explanatory text, Special Publication Series-30, MTA (Mineral Research & Exploration General Directorate), Ankara, Turkey.

Field, E.H. & Group, S.P.I.W., 2000. Accounting for site effects in probabilistic seismic hazard analyses of Southern California: overview of the SCEC Phase III report, *Bull. seism. Soc. Am.,* **90**(6B), S1–S31.

Gözler, M.Z., Cevher, F. & Küçükyaman, A., 1985. Geology and thermal waters of Eskisehir and surroundings, MTA (Mineral Research & Exploration General Directorate) of Turkey Report, Vol. 103(104), pp. 40–50.

Herrmann, R., 2001. *Computer Programs in Seismology-An Overview of Synthetic Seismogram Computation Version 3.1: Department of Earth and Planetary Sciences,* St Louis University.

Horike, M., 1985. Inversion of phase velocity of long-period microtremors to the *S*-wave-velocity structure down to the basement in urbanized areas, *J. Phys. Earth,* **33,** 59–96.

Ibs-von Seht, M. & Wohlenberg, J., 1999. Microtremor measurements used to map thickness of soft sediments, *Bull. seism. Soc. Am.,* **89**(1), 250–259.

Kanai, K., 1961. An Empirical Formula for the Spectrum of Strong Earthquake Motions, *Bull. Earthq. Res. Inst. Univ. Tokyo,* **39,** 85–95

Kanai, K. & Tanaka, T., 1961. On microtremors, *Bull. Earthq. Res. Inst. Univ. Tokyo,* **39**(VIII), 97–115.

Kanai, K., Tanaka, T. & Osada, K., 1954. Measurement of the microtremor I, *Bull. Earthq. Res. Inst. Univ. Tokyo,* **32,** 199–209.

Koçyiğit, A., 2005. The Denizli graben-horst system and the eastern limit of western Anatolian continental extension: basin fill, structure, deformational mode, throw amount and episodic evolutionary history, SW Turkey, *Geodinamica Acta,* **18**(3–4), 167–208.

Koçyiğit, A. & Özacar, A.A., 2003. Extensional neotectonic regime through the NE edge of the outer Isparta Angle, SW Turkey: new field and seismic data, *Turk. J. Earth Sci.*, **12**(1), 67–90.

Köhler, A., Ohrnberger, M., Scherbaum, F., Wathelet, M. & Cornou, C., 2007. Assessing the reliability of the modified three-component spatial autocorrelation technique, *Geophys. J. Int.*, **168**(2), 779–796.

Konno, K. & Ohmachi, T., 1998. Ground-motion characteristics estimated from spectral ratio between horizontal and vertical components of microtremor, *Bull. seism. Soc. Am.*, **88**(1), 228–241.

Kudo, K., 1995. Practical estimates of site response. State-of-the-art report, in *Proceedings of the Fifth International Conference on Seismic Zonation,* Nice, Vol. 1, pp. 17–19.

Lachetl, C. & Bard, P.Y., 1994. Numerical and theoretical investigations on the possibilities and limitations of Nakamura's technique, *J. Phys. Earth,* **42**(5), 377–397.

Lanzo, G. & Silvestri, F., 1999. *Risposta sismica locale: teoria ed esperienze,* Hevelius.

Lermo, J. & Chávez-García, F.J., 1994. Are microtremors useful in site response evaluation, *Bull. seism. Soc. Am.*, **84**(5), 1350–1364.

McKenzie, D., 1972. Active tectonics of the Mediterranean region, *Geophys. J. R. astr. Soc.*, **30**(2), 109–185.

Nakamura, Y., 1989. A method for dynamic characteristics estimation of subsurface using microtremor on the ground surface, *Q. Rep. Railw. Tech. Res. Inst.*, **30**(1), 25–33.

Navarro, M., Enomoto, T., Yamamoto, T., García-Jerez, A., Vidal, F. & Bretón, M., 2008. Analysis of site effects and their correlation with damage distribution observed during the Colima (Mexico) earthquake of January 21, 2003, in *Proceedings of the 14th World Conference on Earthquake Engineering,* Beijing.

Nogoshi, M. & Igarashi, T., 1970. On the propagation characteristics estimations of subsurface using microtremors on the ground surface, *J. Seismol. Soc. Japan,* **23,** 264–280.

Nogoshi, M. & Igarashi, T., 1971. On the amplitude characteristics of microtremor (part 2), *J. Seismol. Soc. Japan,* **24,** 26–40.

Ocakoğlu, F., 2007. A re-evaluation of the Eskişehir Fault Zone as a recent extensional structure in NW Turkey, *J. Asian Earth Sci.*, **31**(2), 91–103.

Ocakoğlu, F. & Açikalin, S., 2010. Field evidences of secondary surface ruptures occurred during the 20 February 1956 Eskişehir earthquake in the NW Anatolia, *J. Earth Syst. Sci.*, **119**(6), 841–851.

Okada, H., 2003. *The Microtremor Survey Method,* Society of Exploration Geophysicists.

Okada, H., 2006. Theory of efficient array observations of microtremors with special reference to the SPAC method, *Explor. Geophys.*, **37**(1), 73–85.

Omori, F., 1908. On micro-tremors, *Bull. Earth Inv. Com.*, **2**(I–II), 1–6.

Orhan, A., Seyrek, E. & Tosun, H., 2007. A probabilistic approach for earthquake hazard ssessment of the Province of Eskisehir, Turkey, *Nat. Hazards Earth Syst. Sci.*, **7,** 607–614.

Ölmez, E., Demirel, Z. & Uzel, Ö.F., 1986. The report of deep borehole data Eskisehir ES-1 and ES 2, Report No: 8142, MTA (Mineral Research & Exploration General Directorate), Ankara, Turkey.

Özalaybey, S., Zor, E., Ergintav, S. & Tapırdamaz, M.C., 2011. Investigation of 3-D basin structures in the İzmit Bay area (Turkey) by single-station microtremor and gravimetric methods, *Geophys. J. Int.*, **186**(2), 883–894.

Park, C.B., Miller, R.D. & Xia, J., 1999. Multichannel analysis of surface waves, *Geophysics,* **64**(3), 800–808.

Parker, E.H., Jr. & Hawman, R.B., 2012. Multi-channel Analysis of Surface Waves (MASW) in karst terrain, southwest Georgia: implications for detecting anomalous features and fracture zones, *J. Environ. Eng. Geophys.*, **17**(3), 129–150.

Parolai, S., Bormann, P. & Milkereit, C., 2002. New relationships between Vs, thickness of sediments, and resonance frequency calculated by the H/V ratio of seismic noise for the Cologne area (Germany), *Bull. seism. Soc. Am.*, **92**(6), 2521–2527.

Parolai, S., Picozzi, M., Richwalski, S. & Milkereit, C., 2005. Joint inversion of phase velocity dispersion and H/V ratio curves from seismic noise recordings using a genetic algorithm, considering higher modes, *Geophys. Res. Lett.*, **32**(1), L01303, doi:10.1029/2004GL021115.

Parolai, S., Ansal, A., Kurtulus, A., Strollo, A., Wang, R. & Zschau, J., 2009. The Ataköy vertical array (Turkey): insights into seismic wave propagation in the shallow-most crustal layers by waveform deconvolution, *Geophysi. J. Int.*, **178**(3), 1649–1662.

Pekkan, E., Tun, M., Guney, Y. & Mutlu, S., 2015. Integrated seismic risk analysis using simple weighting method: the case of residential Eskişehir, Turkey, *Nat. Hazards Earth Syst. Sci.*, **15**(6), 1123–1133.

Sambridge, M., 1999a. Geophysical inversion with a neighbourhood algorithm—I. Searching a parameter space, *Geophys. J. Int.*, **138**(2), 479–494.

Sambridge, M., 1999b. Geophysical inversion with a neighbourhood algorithm-II. Appraising the ensemble, *Geophys. J. Int.*, **138,** 727–746.

Şaroğlu, F., Emre, Ö., Doğan, A. & Yıldırım, C., 2005. Eskisehir fault zone and earthquake, in *Workshop on Eskisehir Fault Zone and Related Systems*, 11 pp.

Sengör, A., Görür, N. & Saroglu, F., 1985. Strike-slip deformation, basin formation and sedimentation: strike-slip faulting and related basin formation in zones of tectonic escape: Turkey as a case study, *Soc. Econ. Paleontol. Mineral., Spec. Pub.*, **37,** 227–264.

Sevinçli, T. & Çatalyürekli, E., 2001. Eskişehir Tepebasi Municipality Geophysics Resistivity Report, General Directorate of State Hydraulic Works.

Seyitoğlu, G., Esat, K., Temel, A. & Telsiz, S., 2010. Determination of main strand of a strike-slip fault by using subsidiary structures: Eskisehir Fault Zone as a case study, in *Tectonic Crossroads: Evolving Orogens of Eurasia-Africa-Arabia,* Abstracts with Programs (8-1), 32 pp.

Seyitoğlu, G. *et al.*, 2015. Determining the main strand of the Eskişehir strike-slip fault zone using subsidiary structures and seismicity: a hypothesis tested by seismic reflection studies, *Turk. J. Earth Sci.*, **24**(1), 1–20.

Tada, T., Cho, I. & Shinozaki, Y., 2009. New circular-array microtremor techniques to infer Love-wave phase velocities, *Bull. seism. Soc. Am.*, **99**(5), 2912–2926.

Tokay, F. & Altunel, E., 2005. Neotectonic activity of Eskişehir fault zone in vicinity of İnönü–Dodurga area, *Bull. Miner. Res. Explor. Inst. Turkey,* **130,** 1–15.

Tokimatsu, K., 1997. Geotechnical site characterization using surface waves, in *Proceedings of 1st International Conference on Earthquake Geotechnical Engineering,* vol. 3, pp. 1333–1368, ed. Ishihara, Balkema.

Tün, M., 2013. Interpretation of ground response and shear-wave velocity (Vs) structure in microzonation studies: a case study in Eskişehir, Istanbul University, *PhD thesis,* Istanbul University, Eskişehir.

Tün, M., Avdan, U., Kaplan, O. & Seyitoğlu, G., 2010. A new look to the Eskişehir Fault, seismic interpretation session 2, no: 43, in *Proceedings of the 19th International Geophysical Congress and Exhibition of Turkey,* Ankara, Turkey.

Wathelet, M., 2005. Array recordings of ambient vibrations: surface-wave inversion, *PhD thesis,* Liège University, Belgium.

Wathelet, M., 2007. *GEOPSY Geophysical Signal Database for Noise Array Processing,* Available at: http://www.geopsy.org/, 2010.

Wathelet, M., 2008. An improved neighborhood algorithm: parameter conditions and dynamic scaling, *Geophys. Res. Lett.*, **35**(9), L09301, doi:10.1029/2008GL033256.

Wathelet, M., Jongmans, D., Ohrnberger, M. & Bonnefoy-Claudet, S., 2008. Array performances for ambient vibrations on a shallow structure and consequences over Vs inversion, *J. Seismol.*, **12**(1), 1–19.

Yaltirak, C., 2002. Tectonic evolution of the Marmara Sea and its surroundings, *Mar. Geol.*, **190**(1), 493–529.